ARTICLES
https://doi.org/10.1038/s41589-020-00689-z
nature chemical biology

Check for updates

SARS-CoV-2 M^{pro} inhibitors and activity-based probes for patient-sample imaging

Wioletta Rut[1]✉, Katarzyna Groborz[1,9], Linlin Zhang[2,3,4,9], Xinyuanyuan Sun[2,3,4], Mikolaj Zmudzinski[1], Bartlomiej Pawlik[5,6], Xinyu Wang[7], Dirk Jochmans[7], Johan Neyts[7], Wojciech Młynarski[5], Rolf Hilgenfeld[2,4,8] and Marcin Drag[1]✉

In December 2019, the first cases of infection with a novel coronavirus, SARS-CoV-2, were diagnosed. Currently, there is no effective antiviral treatment for COVID-19. To address this emerging problem, we focused on the SARS-CoV-2 main protease that constitutes one of the most attractive antiviral drug targets. We have synthesized a combinatorial library of fluorogenic substrates with glutamine in the P1 position. We used it to determine the substrate preferences of the SARS-CoV and SARS-CoV-2 main proteases. On the basis of these findings, we designed and synthesized a potent SARS-CoV-2 inhibitor (Ac-Abu-D-Tyr-Leu-Gln-VS, half-maximal effective concentration of 3.7 μM) and two activity-based probes, for one of which we determined the crystal structure of its complex with the SARS-CoV-2 M^{pro}. We visualized active SARS-CoV-2 M^{pro} in nasopharyngeal epithelial cells of patients suffering from COVID-19 infection. The results of our work provide a structural framework for the design of inhibitors as antiviral agents and/or diagnostic tests.

In December 2019, a severe respiratory disease of unknown origin emerged in Wuhan, Hubei province, China[1,2]. Symptoms of the first patients were flu-like and included fever, cough and myalgia, but with a tendency to develop a potentially fatal dyspnea and acute respiratory distress syndrome[2]. Genetic analysis confirmed a betacoronavirus as the causing agent. The virus was initially named 2019 novel coronavirus (2019-nCoV)[1–3], but shortly thereafter, it was renamed SARS-CoV-2 (ref. [4]). By 28 August 2020, the World Health Organization had registered >24 million cumulative cases of coronavirus disease 2019 (COVID-19), with 836,475 deaths[5].

Currently, there is no approved vaccine or treatment for COVID-19. Efforts are being made to characterize molecular targets, pivotal for the development of anticoronaviral therapies[6]. The main protease (M^{pro}, also known as 3CL^{pro}), is one of the coronavirus nonstructural proteins (Nsp5) designated as a potential target for drug development[7,8]. M^{pro} cleaves the viral polyproteins, generating 12 nonstructural proteins (Nsp4-Nsp16), including the RNA-dependent RNA polymerase (RdRp, Nsp12) and the helicase (Nsp13). Inhibition of M^{pro} would prevent the virus from replication and therefore constitutes one of the potential anticoronaviral strategies[7–9].

Due to the close phylogenetic relationship between SARS-CoV-2 and SARS-CoV[3,10,11], their main proteases share many structural and functional features. From the perspective of the design and synthesis of new M^{pro} inhibitors, a key feature of both the enzymes is their ability to cleave the peptide bond following Gln. The SARS-CoV M^{pro} cleaves polyproteins mainly within the Leu-Gln↓(Ser, Ala, Gly) sequence (↓ indicates the cleavage site), which appears to be a preferred pattern of this protease[7,9,12]. The specificity for peptide bond hydrolysis after Gln residues is also observed for main proteases of other coronaviruses[13,14] but is rare for human enzymes. This observation, along with further studies on the M^{pro}, can potentially lead to new broad-spectrum anticoronaviral inhibitors with minimal side effects[15].

In the present study, we applied the HyCoSuL (hybrid combinatorial substrate library) approach to determine the full substrate specificity profile of SARS-CoV and SARS-CoV-2 M^{pro}s. The use of natural and a large number of unnatural amino acids with diverse chemical structures allowed an in-depth characterization of the residue preference of the binding pockets within the substrate-binding site of the proteases. The results from library screening enabled us to design and synthesize ACC-labeled substrates with improved catalytic efficiency in comparison to a substrate containing only natural amino acids. Moreover, results from our studies clearly indicate that SARS-CoV M^{pro} and SARS-CoV-2 M^{pro} exhibit highly overlapping substrate specificities. We have used this knowledge to design activity-based probes (ABPs) specific for the SARS-CoV main proteases as well as tetrapeptide inhibitors. Further, we present a crystal structure of the SARS-CoV-2 M^{pro} in complex with one of the ABPs. Finally, using the ABP, we were able to visualize active SARS-CoV-2 M^{pro} within nasopharyngeal epithelial cells of patients with active COVID-19 infection. These data provide a useful basis for the design of chemical compounds for effective diagnosis and therapy of COVID-19.

Results

Substrate specificity of SARS-CoV and SARS-CoV-2 M^{pro}s. To determine the SARS-CoV M^{pro} and SARS-CoV-2 M^{pro} substrate preferences, we applied a HyCoSuL approach. The library consists of

[1]Department of Chemical Biology and Bioimaging, Wroclaw University of Science and Technology, Wroclaw, Poland. [2]Institute of Molecular Medicine, University of Lübeck, Lübeck, Germany. [3]Institute of Biochemistry, Center for Structural and Cell Biology in Medicine, University of Lübeck, Lübeck, Germany. [4]German Center for Infection Research (DZIF), Hamburg-Lübeck-Borstel-Riems Site, University of Lübeck, Lübeck, Germany. [5]Department of Pediatrics, Oncology & Hematology, Medical University of Lodz, Lodz, Poland. [6]Postgraduate School of Molecular Medicine, Medical University of Warsaw, Warsaw, Poland. [7]Laboratory of Virology and Chemotherapy, Department of Microbiology, Immunology and Transplantation, Rega Institute, KU Leuven, Leuven, Belgium. [8]Center for Brain, Behavior, and Metabolism, University of Lübeck, Lübeck, Germany. [9]These authors contributed equally: Katarzyna Groborz, Linlin Zhang ✉e-mail: wioletta.rut@pwr.edu.pl; marcin.drag@pwr.edu.pl

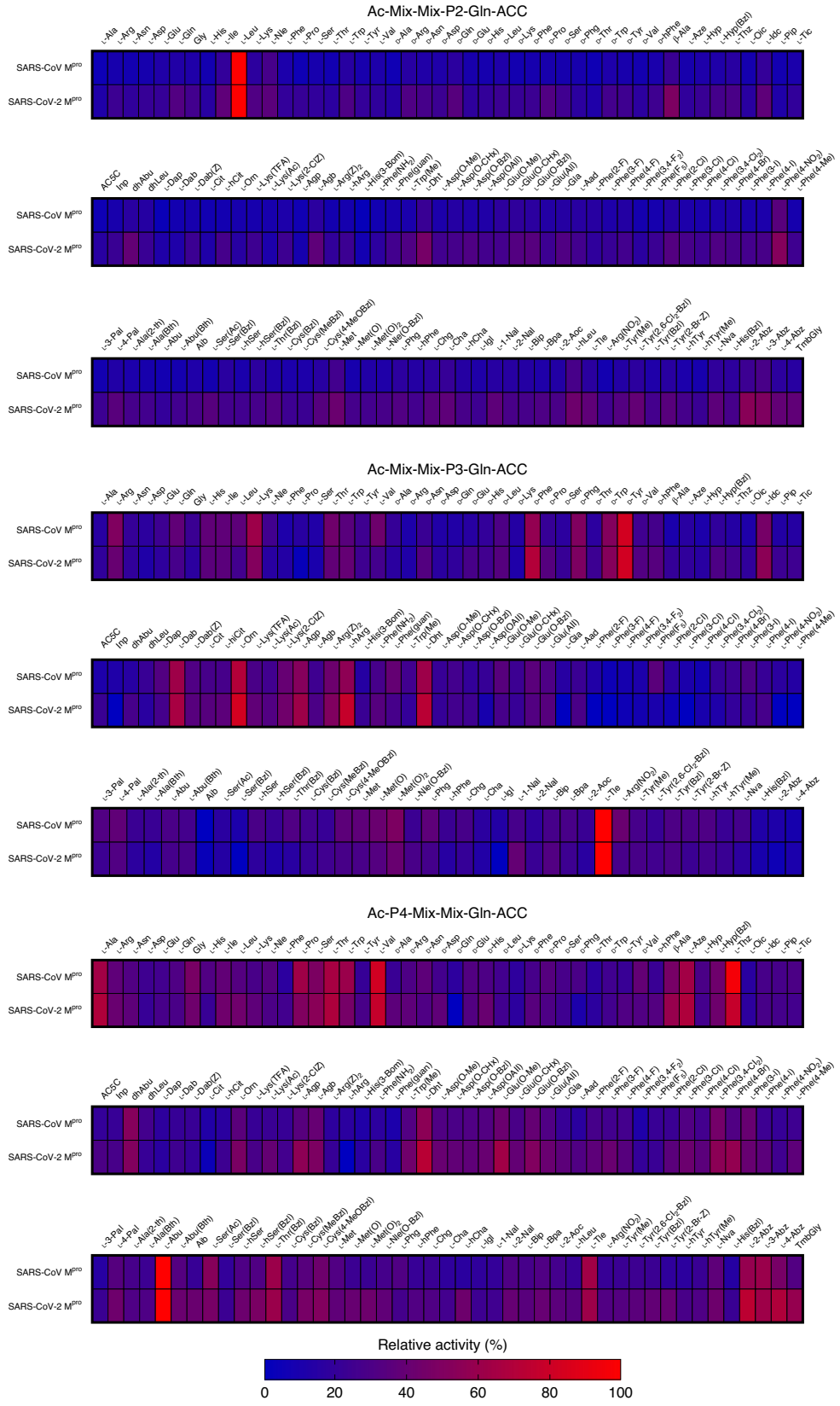

Fig. 1 | Substrate specificity profiles of SARS-CoV M^{pro} and SARS-CoV-2 M^{pro} presented as heat maps. The average relative activity is presented as a percentage of the best-recognized amino acid ($n = 2$, where n represents the number of independent experiments).

three sublibraries, each of them comprising a fluorescent tag, ACC (7-amino-4-carbamoylmethylcoumarin); two fixed positions and two varied positions containing an equimolar mixture of 19 amino acids (Mix) (P2 sublibrary, Ac-Mix-Mix-X-Gln-ACC; P3 sublibrary, Ac-Mix-X-Mix-Gln-ACC; P4 sublibrary, Ac-X-Mix-Mix-Gln-ACC, X = 19 natural and over 100 unnatural amino acids, Extended Data

Table 1 | Kinetic parameters of selected substrates for SARS-CoV-2 M^{pro}

Substrate	K_M (μM)	k_{cat} (s^{-1})	k_{cat}/K_M ($M^{-1}s^{-1}$)
Ac-Abu-Tle-Leu-Gln-ACC, QS1 (**1**)	207.3 ± 12.0	0.178 ± 0.016	859 ± 57
Ac-Thz-Tle-Leu-Gln-ACC, QS4 (**2**)	189.5 ± 2.7	0.144 ± 0.006	760 ± 50
Ac-Val-Lys-Leu-Gln-ACC, QS2 (**3**)	228.4 ± 9.9	0.050 ± 0.002	219 ± 3

Data presented as mean values ± s.d.; $n = 3$, where n represents the number of independent experiments.

Fig. 1). We incorporated glutamine at the P1 position, because the available crystal structures of SARS-CoV M^{pro} revealed that only glutamine (and, at only one cleavage site, histidine) can occupy the S1 pocket of this enzyme[12,16]. The imidazole of His163, located near the bottom of the S1 pocket, is suitably positioned to interact with the Gln side chain. The Gln is also involved in two other interactions; that is, with the main chain of Phe140 and the side chain of Glu166. The library screen revealed that SARS-CoV and SARS-CoV-2 M^{pro} display very similar substrate specificities (Fig. 1). The most preferred amino acid at the P2 position is leucine in the case of both proteases. SARS-CoV M^{pro} exhibits lower activity toward other tested amino acids at this position (<30%). Leu selectivity for SARS-CoV M^{pro} is in high agreement with a previous report by Zhu et al.[17]. However, we have noticed some discrepancies in the level of selectivity for other natural amino acids. This is the result of differences in the substrate specificity profiling approach, where we are using a combinatorial mixture of natural amino acids, while Zhu et al. were using a defined peptide sequence. Nevertheless, in both approaches, preferences for the same natural amino acids were observed. The S2 pocket of both investigated enzymes can accommodate other hydrophobic residues, such as 2-Abz, Phe(4-NO_2), 3-Abz, β-Ala, Dht, hLeu, Met and Ile (amino-acid structures are presented in Supplementary Table 1). At the P3 position, both enzymes prefer hydrophobic D and L amino acids and also positively charged residues; the best are Tle, D-Phe, D-Tyr, Orn, hArg, Dab, Dht, Lys, D-Phg, D-Trp, Arg and Met(O)$_2$. At the P4 position, SARS-CoV and SARS-CoV-2 M^{pro} possess broad substrate specificity. The most preferred are small aliphatic residues such as Abu, Val, Ala and Tle, but other hydrophobic amino acids are also accepted. These findings can be partly explained by the available crystal structures of SARS-CoV M^{pro} in complex with inhibitors[8,12,16]. The hydrophobic S2 subsite of SARS-CoV M^{pro} is more flexible compared to alphacoronavirus M^{pro}s, which explains the less stringent specificity[15]. The S2 pocket can form hydrophobic interactions with P2 residues that are not only limited to leucine. The S3 pocket of SARS-CoV M^{pro} is not well defined, which is also reflected by our P3 substrate specificity profile. The S4 pocket can be occupied by small residues due to the crowded cavity formed by Leu167, Pro168 at the bottom and Thr190, Ala191 at the top wall.

To validate the results from library screening, we designed and synthesized ACC-labeled substrates containing the most preferred amino acids in each position. Then, we measured the rate of substrate hydrolysis (chemical compounds **1**–**8**) relevant to each protease (Extended Data Fig. 2). The data clearly demonstrate that SARS-CoV M^{pro} and SARS-CoV-2 M^{pro} exhibit the same activity toward tested substrates. The results are consistent with the HyCoSuL screening data. The most preferred substrate, Ac-Abu-Tle-Leu-Gln-ACC (**1**), is composed of the best amino acids in each position (Supplementary Table 2). Kinetic parameters were determined for the two best substrates (Ac-Abu-Tle-Leu-Gln-ACC, **1**; Ac-Thz-Tle-Leu-Gln-ACC, **2**) and one containing the best-recognized natural amino acids (Ac-Val-Lys-Leu-Gln-ACC, **3**) (Table 1 and Extended Data Fig. 3) toward SARS-CoV-2 M^{pro}. Due to substrate precipitation because of high concentration needed in the assay, kinetic parameters toward SARS-CoV M^{pro} could not be determined. Analysis of kinetic parameters revealed that these three substrates differ in the k_{cat} value, while K_M values are comparable. Since SARS-CoV-2 M^{pro} exhibits low activity toward tetrapeptide substrates, we synthesized internally quenched fluorescent substrates (IQF) containing the same amino acids at the P4-P1 positions as substrates QS1, QS2 and QS4. The general sequence of IQF substrates was derived from the N-terminal autocleavage sequence of the viral protease reported previously (MCA-AVLQSGFRK (Dnp)K)[18]; instead of the MCA fluorophore, ACC was used. We also incorporated a small linker (glycine residue) between ACC and the amino acid at the P4 position for efficient synthesis. Specificity constant values (k_{cat}/K_M) for these IQF substrates were much higher than for tetrapeptide substrates. IQF substrates containing the same amino acids at P4-P1 positions as substrates QS1 (ACC-Gly-Abu-Tle-Leu-Gln-Ser-Gly-Phe-Arg-Lys(dnp)-Lys-NH_2,**9**) and QS4 (ACC-Gly-Thz-Tle-Leu-Gln-Ser-Gly-Phe-Arg-Lys(dnp)-Lys-NH_2, **10**) were better recognized than the IQF substrate possessing the same peptide sequence as the QS2 (ACC-Gly-Val-Lys-Leu-Gln-Ser-Gly-Phe-Arg-Lys(dnp)-Lys-NH_2, **11**) substrate (Supplementary Table 3). This is in line with kinetic results obtained for tetrapeptide substrates.

Inhibitors and ABPs of SARS-CoV-2 M^{pro}. In the next step, the best substrate QS1 was converted into an inhibitor and ABPs. The inhibitor contained the acetylated peptide sequence and vinyl sulfone as an irreversible reactive group (Ac-Abu-Tle-Leu-Gln-VS, Ac-QS1-VS (**12**), Fig. 2a). The probes included an N-terminal biotin tag (B) or the Cyanine 5 dye (Cy5), polyethylene glycol (PEG(4)) as a linker, the best peptide sequence and vinyl sulfone (Fig. 2a, and Extended Data Fig. 4a). To evaluate the sensitivity of the designed probes, we performed SDS–PAGE analysis followed by protein transfer onto membranes and ABP visualization. We observed SARS-CoV-2 M^{pro} (100 nM) labeling by B-QS1-VS (**13**) at a concentration of 200 nM and by Cy5-QS1-VS (**14**) at 100 nM (Fig. 2b

Fig. 2 | SARS-CoV-2 M^{pro} detection by ABPs. a, Structure of inhibitors and ABPs. **b**–**d**, SARS-CoV-2 M^{pro} labeling by probes B-QS1-VS (**b**) and Bodipy-QS5-VS) (**c**). **c**, SARS-CoV-2 M^{pro} (5, 10, and 50 nM) was detected by different concentrations of Bodipy-QS5-VS. **d**, Time-point analysis of Bodipy-QS5-VS binding to the enzyme. **e**, SARS-CoV-2 M^{pro} probe selectivity in HeLa and HEK-293T lysates (asterisk shows the SARS-CoV-2 M^{pro}, which was spiked into the cell lysates). The cell lysate was incubated with or without the inhibitor Ac-QS5-VS for 30 min at 37 °C; next, different probe concentrations were added and the samples were incubated for 30 min at 37 °C. The biotinylated ABP was detected with a fluorescent streptavidin Alexa Fluor 647 conjugate (1:10,000) in TBS-T with 1% BSA using an Azure Biosystems Sapphire Biomolecular Imager (laser 658 and 488 nm for Bodipy FL dye) and the Azure Spot Analysis software. Each experiment was repeated independently two times with similar results. **f**,**g**, Antiviral activity on SARS-CoV-2 (**f**) and cellular toxicity (**g**) in Huh7 cells of Ac-Abu-DTyr-Leu-Gln-VS and GS-441524. Antiviral activity and toxicity was determined by quantification of viability of infected (**f**) or uninfected (**g**) cell cultures (see Methods). Two independent dose–response curves were investigated for each compound (indicated by the circles and triangels). Nonlinear fitting of the dose–response curves results in EC_{50}s of 1.2 and 1.3 μM for GS-441524 and 3.5 and 4.0 μM for Ac-Abu-DTyr-Leu-Gln-VS. Calculated CC_{50}s are 69 and 95 μM for GS-441524 and >100 μM for Ac-Abu-DTyr-Leu-Gln-VS.

and Extended Data Fig. 4b) that reflected the results of the k_{obs}/I (I, inhibitor or probe concentration) analysis (Table 2 and Extended Data Fig. 5). In our previous studies, we showed that an ABP with low potency can be applied to detect protease activity in cell assays[19]. To determine the probe selectivity, we performed cell lysate assays. A HeLa lysate was incubated with different probe concentrations (50, 100 and 200 nM) (Extended Data Fig. 4c). The cell lysate experiment confirmed probe selectivity. To verify that unknown bands (about 30 kDa and between 49 and 62 kDa) were due to unspecific Cy5 labeling, we incubated the cell lysate with inhibitor (Ac-QS1-VS)

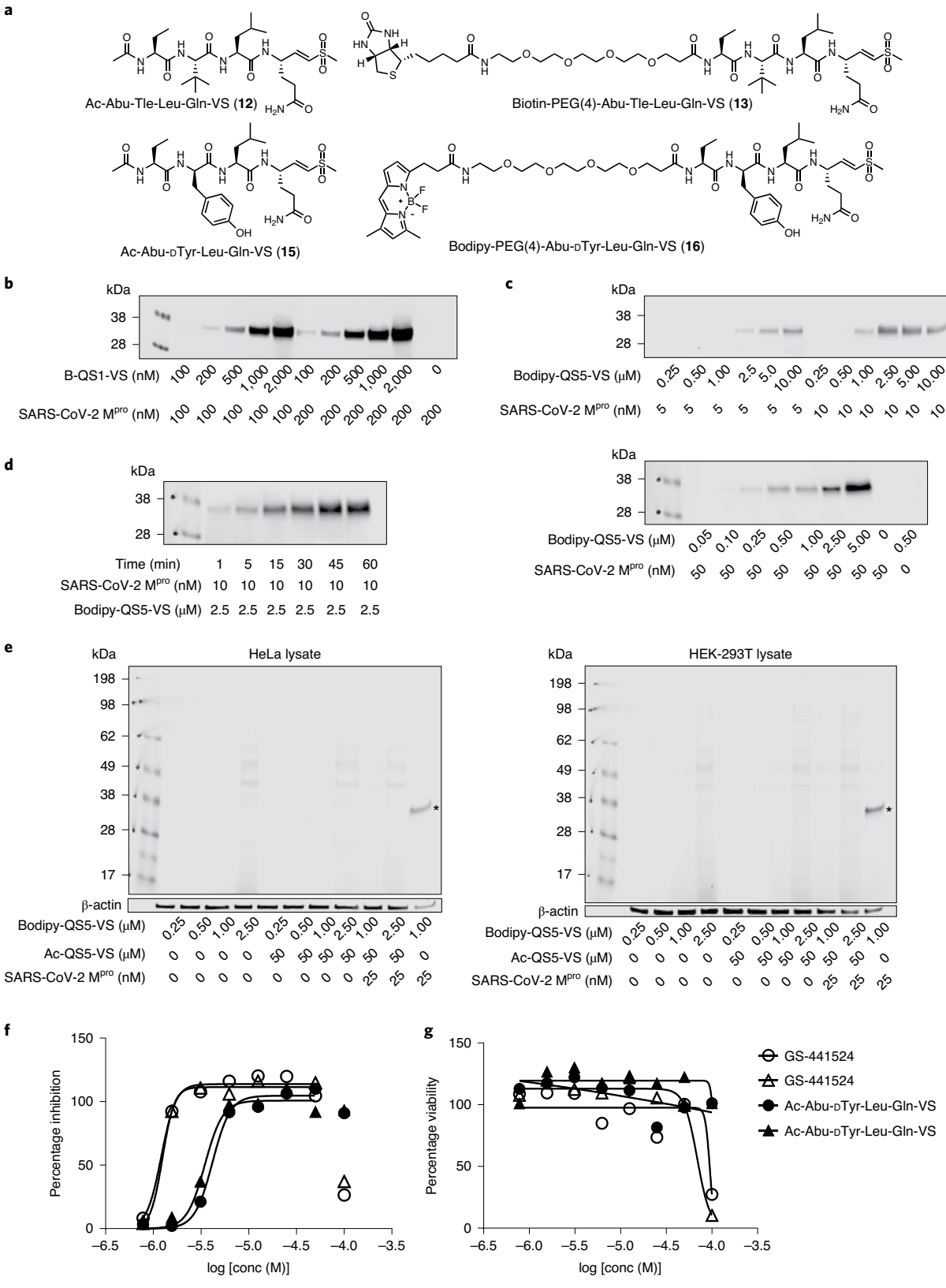

Table 2 | Inhibition rate constants of SARS-CoV-2 M^{pro} for inhibitors and ABPs

Compound	k_{obs}/I ($M^{-1}s^{-1}$)
Ac-Abu-Tle-Leu-Gln-VS, Ac-QS1-VS (**12**)	730 ± 17
Biotin-PEG(4)-Abu-Tle-Leu-Gln-VS, B-QS1-VS (**13**)	200 ± 11
Cy5-PEG(4)-Abu-Tle-Leu-Gln-VS, Cy5-QS1-VS (**14**)	591 ± 45
Ac-Abu-DTyr-Leu-Gln-VS, Ac-QS5-VS (**15**)	812 ± 70
Bodipy-PEG(4)-Abu-DTyr-Leu-Gln-VS, Bodipy-QS5-VS (**16**)	439 ± 34

Data presented as mean values ± s.d.; $n = 3$, where n represents the number of independent experiments.

for 30 min at 37 °C and then with Cy5-QS1-VS for 15 min at 37 °C (lanes 8–10 on the membrane, Extended Data Fig. 4c). The same protein bands were observed on the membrane when cell lysates were incubated with and without Ac-QS1-VS, which confirmed unspecific protein labeling by the Cy5 dye. Due to this unspecific protein labeling by Cy5-QS1-VS, we decided to slightly modify the probe structure. Since amino acids with D-stereochemistry are not recognized by many human proteases[20–23], we changed Tle at the P3 position to D-Tyr, which is well recognized by SARS-CoV-2 M^{pro} at this position, to improve probe selectivity. The Cy5 fluorophore was exchanged to the Bodipy FL fluorophore. The designed inhibitor (Ac-Abu-DTyr-Leu-Gln-VS, Ac-QS5-VS, **15**) and the ABP (Bodipy-PEG(4)-Abu-DTyr-Leu-Gln-VS, Bodipy-QS5-VS, **16**) were tested on the recombinant enzyme and cell lysates (Fig. 2). Kinetic analysis revealed that Ac-QS5-VS exhibited the same potency toward SARS-CoV-2 M^{pro} as Ac-QS1-VS (Table 2). The designed ABP, Bodipy-QS5-VS, was slightly less active toward the main protease than Cy5-QS1-VS. To assess Bodipy-QS5-VS sensitivity, we incubated SARS-CoV-2 M^{pro} (at three different concentrations of 5, 10 and 50 nM) with different probe concentrations for 30 min. We observed the detection of SARS-CoV-2 M^{pro} at 5 nM by 2.5 μM Bodipy-QS5-VS (Fig. 2c). The enzyme labeling by the ABP is noticeable after 5 min of incubation (Fig. 2d). Cell lysate assays (HeLa and human embryonic kidney (HEK)-293T) confirmed Bodipy-QS5-VS selectivity (Fig. 2e). Ac-Abu-DTyr-Leu-Gln-VS was also tested for its antiviral activity using a fully replication-competent SARS-CoV-2 strain in Huh7 cell culture. Here the inhibitor showed selective inhibition (half-maximal effective concentration (EC_{50}) = 3.7 μM; interquartile range (IQR) 3.5–4.0 μM) with no notable toxicity (50% cytotoxic concentration (CC_{50}) > 100 μM). As a comparison, the parent nucleoside of remdesivir (GS-441524) under the same conditions showed an EC_{50} of 1.15 μM (IQR 1.1–1.2 μM) and a CC_{50} of 87 μM (IQR 82–92 μM) (Fig. 2f,g).

Crystal structure of SARS-CoV-2 M^{pro} with B-QS1-VS. To visualize the steric details of the interactions between the M^{pro} and the ABP, Biotin-PEG(4)-Abu-Tle-Leu-Gln-VS (B-QS1-VS), we determined the X-ray crystal structure of the complex between the two components. The probe was cocrystallized with the recombinant and highly purified SARS-CoV-2 M^{pro}. Crystals diffracted to 1.7 Å resolution and were of space group $P6_122$, with one ABP-M^{pro} monomer per asymmetric unit (see Supplementary Table 4 for crystallographic details). The structure was refined to reasonable R factors and good geometry. Most of the atoms of the ABP were clearly seen in the $2F_o–F_c$ electron density (F_o, observed structure factor amplitudes; F_c, structure factor amplitudes calculated from the model) at a contour level of 0.5σ. The reason for this is that the flexible tail of the ABP, the PEG(4) chain and the terminal biotin label, are in contact with a neighboring M^{pro} dimer in the crystal lattice (Extended Data Fig. 6a). This is of course of little relevance for the situation in solution; hence we discuss only the interaction of the P4-P1 residues with the parent M^{pro} molecule (Fig. 3) here. The oxygen atoms of the vinyl sulfone group point toward the oxyanion hole of the protease and accept hydrogen bonds (2.81 and 3.26 Å) from the main-chain amide groups of Gly143 and Cys145, respectively. Also, the side-chain amide nitrogen of Asn142 donates a 2.90-Å hydrogen bond (H bond) to one of these oxygens. The methyl group attached to the sulfone makes hydrophobic contacts with the Cγ2 atom of Thr25 and the side chain of Leu27, within the S1' subsite. The catalytic cysteine residue is covalently linked to the Cβ atom of the vinyl group, at a distance of 1.83 Å.

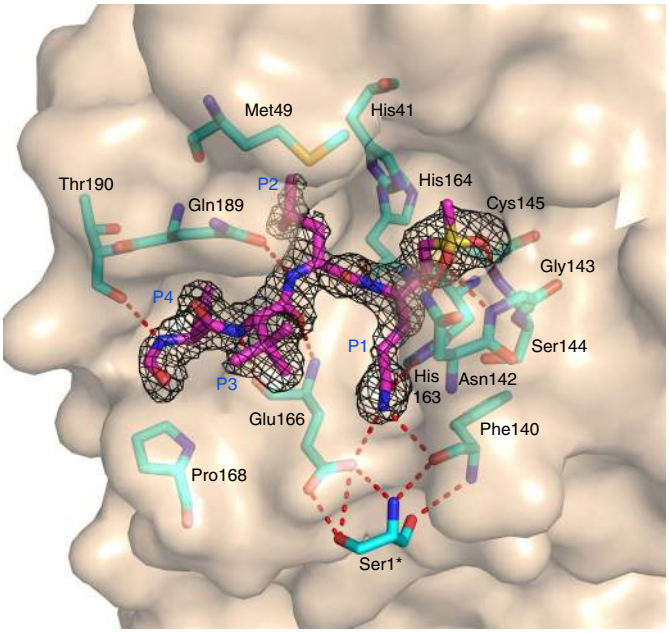

Fig. 3 | Three-dimensional structure of the P4-P1′ residues of the ABP Biotin-PEG(4)-Abu-Tle-Leu-Gln-VS (B-QS1-VS) in the substrate-binding site of the SARS-CoV-2 M^{pro}. The $F_o–F_c$ electron density for residues P4-P1′ of the ABP is shown at a contour level of 2.5σ. All parts of the ABP beyond the P4 residue would be outside the parent M^{pro} dimer and have been omitted from this figure. However, the rest of the ABP interacts with a neighboring M^{pro} dimer in the crystal (Extended Data Fig. 6a) and is seen in the electron density maps.

The P1-glutamine side chain makes the expected interaction with His163 (2.72 Å, through the Oε1 atom) and the Phe140 main-chain oxygen (3.22 Å, through Nε2) and Glu166 Oε1 (3.25 Å). The Nε2 of the P1-Gln thus donates a three-center (bifurcated) hydrogen bond to these two acceptors. This is also reflected in inhibitors that carry a γ-lactam as Gln surrogate in the P1 position, such as compound 13b (ref. [9]). The Leu residue in the S2 pocket makes the canonical interactions previously observed[17], with residues Met49, Met165, His41 and the Cα atom of Arg188. Also, the main-chain amide of the P2-Leu donates a 2.98-Å H bond to the side chain Oε1 of Gln189.

There is no well-defined pocket for the P3 moiety, which is therefore mostly solvent-exposed. There may be some weak interaction of the Tle side chain with the hydrophobic portion of the neighboring Glu166 side chain. The polar main-chain atoms of the P3 residue form hydrogen bonds with the protein main chain at Glu166. The aminobutyric acid in P4 makes weak hydrophobic interactions with Leu167 and Gln189, and its main-chain NH group donates a H bond to Thr190 O.

We have previously noticed that compared to the SARS-CoV M^{pro}, Thr285 has been replaced by Ala in SARS-CoV-2 M^{pro}

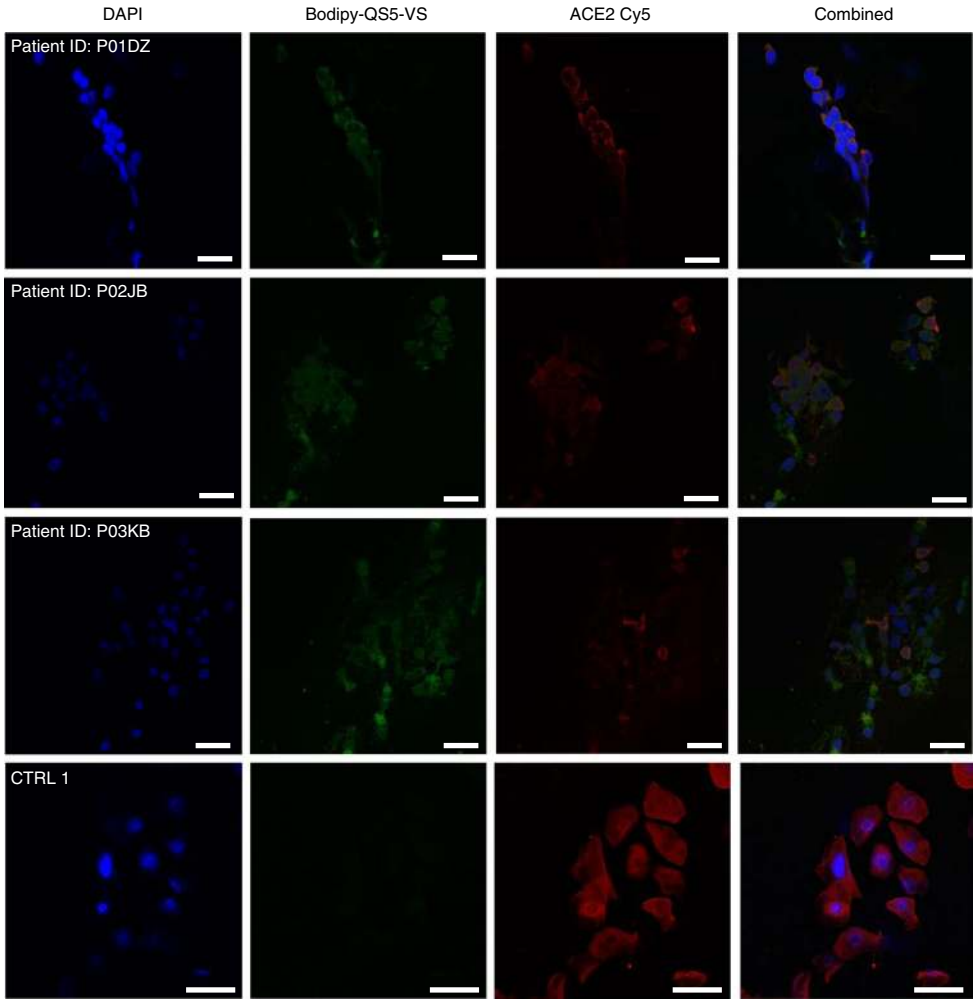

Fig. 4 | SARS-CoV-2 M^{pro} detection by the ABP Bodipy-QS5-VS in nasopharyngeal epithelial cells from patients who tested positive for SARS-CoV-2 RNA and from a healthy control. Confocal microscopy of the epithelial cells of nasopharyngeal swabs co-stained with Bodipy-QS5-VS SARS-CoV-2 M^{pro} probe and anti-ACE2 antibody (ACE2, angiotensin-converting enzyme 2) with Cy5 AffiniPure donkey anti-Goat secondary antibody and DAPI. Due to ethical concerns, one nasopharyngeal swab was collected from each patient. Cells come from the following patients who tested positive: P01DZ, P02JB and P03KB and a control (CTRL). Scale bars, 25 µm. Control 1; scale bars, 50 µm.

and the neighboring Ile286 by Leu[9]. In the SARS-CoV M^{pro}, the Thr285 makes a hydrogen bond with its symmetry-mate across the twofold axis creating the M^{pro} dimer. The loss of this H bond in the SARS-CoV-2 M^{pro} enables the monomers of the dimer to approach each other more closely. In the crystal structure presented here, the space between the two protomers generated by the mutation is filled by a chloride ion adopted from the crystallization buffer (Extended Data Fig. 6b). This might be taken as a hint for this region around residues 284–286 being a hotspot for mutations, due to nonideal packing of the two protomers of the dimer at this point.

SARS-CoV-2 M^{pro} detection and imaging in patient samples. Fluorescent-tagged ABPs currently represent the classic standard in terms of application for labeling of biological samples and have been successfully used for visualization of many proteases in the past[24–26]. We wanted to see if the Cy5-QS1-VS developed by us can be used for detection of SARS-CoV-2 M^{pro} in human samples. Thus, we recruited one patient with mild symptoms of COVID-19, who was positive for SARS-CoV-2 RNA in two independent quantitative PCR with reverse transcription assays validated for diagnostic purposes. We incubated the probe at final concentration of 1 µM with cells collected from nasopharyngeal swabs of the patient on the first and fifth days after diagnosis and subjected them to confocal laser scanning microscopy. In parallel, we carried out the same experiment with a healthy donor (COVID-19-negative control). These serial measurements revealed that 10–15% of the cells were positive for staining with the Cy5-QS1-VS probe in the patient who tested positive for COVID-19 (Extended Data Fig. 7). A particularly strong signal from SARS-CoV-2 M^{pro} was observed on the fifth day after diagnosis. No signal from SARS-CoV-2 M^{pro} labeling was observed in the sample from the healthy donor (Extended Data Fig. 7). Due to a noticeable background fluorescence signal from the Cy5 dye in the control sample (negative for COVID-19), we changed the probe structure and performed the same experiments using a new probe, Bodipy-QS5-VS, among additional six patients positive for SARS-CoV-2 RNA with clinical signs of COVID-19 and three negative, healthy individuals (control samples). We observed labeling of SARS-CoV-2 M^{pro} in the patients positive for COVID-19 by Bodipy-QS5-VS and no signal from the probe in the patients who tested negative (Fig. 4 and Extended Data Fig. 8a,c). When the cells (samples positive for COVID-19) were incubated with Ac-QS1-VS inhibitor before the Bodipy-QS5-VS probe, SARS-CoV-2 M^{pro} staining was reduced (Extended Data Fig. 8b). Thus, we were able to show that human cells collected ex vivo contain active SARS-CoV-2 M^{pro} during SARS-CoV-2 infection.

Discussion

SARS-CoV-2, first observed in Wuhan, China, caused the current pandemic of COVID-19 disease. The lack of a vaccine or approved medications for direct treatment of the disease has led to strenuous efforts to find therapies and stop the pandemic. Among the promising therapeutic targets are two viral proteases: SARS-CoV-2 M^{pro} and SARS-CoV-2 PL^{pro}. The first, SARS-CoV-2 M^{pro}, is used by the virus for protein maturation and its structure has been recently described[9]. Moreover, the results of retargeting about 10,000 drugs, drug candidates in clinical trials and other bioactive compounds resulted in selection of several candidates as potential inhibitors of this enzyme[18]. In our research, we decided to thoroughly examine SARS-CoV-2 M^{pro} to find the optimal chemical tools in the form of substrates, inhibitors and ABPs. First, we obtained a targeted library of fluorogenic substrates (HyCoSuL) toward this protease and determined the substrate specificity at the P4-P2 positions. We directly compared the substrate specificity of the main protease with the same protease from the previous SARS coronavirus, which caused an epidemic in 2003. Our data clearly demonstrate that these enzymes have very similar preferences for natural and unnatural amino acids at the P4-P2 positions. They tolerate many different amino acids at P4 and P3, and have a strong preference for Leu at P2. This information is certainly crucial for the aspect of drug retargeting, but so is the use of information obtained in previous years for SARS-CoV M^{pro} to be used for current research. In the next step, we created potent inhibitors and ABPs with sequences based on the HyCoSuL screening results. This strategy had been successfully applied in our previous studies to design selective inhibitors and ABPs for cysteine[24,27], serine[22] and threonine[23] proteases. In the case of B-QS1-VS, we also obtained a crystal structure of its complex with SARS-CoV-2 M^{pro}, which accurately shows the binding mechanism in the P4-P1' pockets. This knowledge certainly complements the information already obtained for other inhibitor molecules published for this enzyme. In turn, we used the fluorescent ABP to visualize the SARS-CoV-2 M^{pro} activity in patient samples with COVID-19, thus confirming that it is an excellent tool that can be used to detect this enzyme and can also be used as a diagnostic tool.

In conclusion, our research allowed for the exact characterization of SARS-CoV-2 M^{pro} in terms of both aminoacid preferences as well as the design of targeted inhibitors and ABPs. The reagents described here can be used to optimize structures that lead to anti-COVID-19 drugs, as well as for further drug retargeting.

Online content

Any methods, additional references, Nature Research reporting summaries, source data, extended data, supplementary information, acknowledgements, peer review information; details of author contributions and competing interests; and statements of data and code availability are available at https://doi.org/10.1038/s41589-020-00689-z.

Received: 3 June 2020; Accepted: 5 October 2020;
Published online: 22 October 2020

References

1. Wang, C., Horby, P. W., Hayden, F. G. & Gao, G. F. A novel coronavirus outbreak of global health concern. *Lancet* **395**, 470–473 (2020).
2. Huang, C. L. et al. Clinical features of patients infected with 2019 novel coronavirus in Wuhan, China. *Lancet* **395**, 497–506 (2020).
3. Wu, F. et al. A new coronavirus associated with human respiratory disease in China. *Nature* **579**, 265–269 (2020).
4. Jiang, S. B. et al. A distinct name is needed for the new coronavirus. *Lancet* **395**, 949–949 (2020).
5. *Coronavirus Disease (COVID-2019) Situation Reports, 5 August 2020* https://www.who.int/docs/default-source/coronaviruse/situation-reports/20200805-covid-19-sitrep-198.pdf?sfvrsn=f99d1754_2 (WHO, 2020).
6. Li, G. D. & De Clercq, E. Therapeutic options for the 2019 novel coronavirus (2019-nCoV). *Nat. Rev. Drug Discov.* **19**, 149–150 (2020).
7. Hilgenfeld, R. From SARS to MERS: crystallographic studies on coronaviral proteases enable antiviral drug design. *FEBS J.* **281**, 4085–4096 (2014).
8. Pillaiyar, T., Manickam, M., Namasivayam, V., Hayashi, Y. & Jung, S. H. An overview of severe acute respiratory syndrome-coronavirus (SARS-CoV) 3CL protease inhibitors: peptidomimetics and small molecule chemotherapy. *J. Med. Chem.* **59**, 6595–6628 (2016).
9. Zhang, L. L. et al. Crystal structure of SARS-CoV-2 main protease provides a basis for design of improved alpha-ketoamide inhibitors. *Science* **368**, 409–412 (2020).
10. Wu, A. P. et al. Genome composition and divergence of the novel coronavirus (2019-nCoV) originating in China. *Cell Host Microbe* **27**, 325–328 (2020).
11. Zhou, P. et al. A pneumonia outbreak associated with a new coronavirus of probable bat origin. *Nature* **579**, 270–273 (2020).
12. Anand, K., Ziebuhr, J., Wadhwani, P., Mesters, J. R. & Hilgenfeld, R. Coronavirus main proteinase (3CL(pro)) structure: basis for design of anti-SARS drugs. *Science* **300**, 1763–1767 (2003).
13. Wu, A. D. et al. Prediction and biochemical analysis of putative cleavage sites of the 3C-like protease of Middle East respiratory syndrome coronavirus. *Virus Res.* **208**, 56–65 (2015).
14. Chuck, C. P., Chow, H. F., Wan, D. C. C. & Wong, K. B. Profiling of substrate specificities of 3C-like proteases from group 1, 2a, 2b, and 3 coronaviruses. *PloS ONE* **6**, https://doi.org/10.1371/journal.pone.0027228 (2011).
15. Zhang, L. L. et al. alpha-Ketoamides as broad-spectrum inhibitors of coronavirus and enterovirus replication: structure-based design, synthesis, and activity assessment. *J. Med. Chem.* **63**, 4562–4578 (2020).
16. Yang, H. T. et al. The crystal structures of severe acute respiratory syndrome virus main protease and its complex with an inhibitor. *Proc. Natl Acad. Sci. USA* **100**, 13190–13195 (2003).
17. Zhu, L. L. et al. Peptide aldehyde inhibitors challenge the substrate specificity of the SARS-coronavirus main protease. *Antivir. Res.* **92**, 204–212 (2011).
18. Jin, Z. M. et al. Structure of M-pro from SARS-CoV-2 and discovery of its inhibitors. *Nature* **582**, 289–293 (2020).
19. Aleshin, A. E. et al. Activity, specificity, and probe design for the smallpox virus protease K7L. *J. Biol. Chem.* **287**, 39470–39479 (2012).
20. Poreba, M. et al. Unnatural amino acids increase sensitivity and provide for the design of highly selective caspase substrates. *Cell Death Differ.* **21**, 1482–1492 (2014).
21. Kasperkiewicz, P. et al. Design of ultrasensitive probes for human neutrophil elastase through hybrid combinatorial substrate library profiling. *Proc. Natl Acad. Sci. USA* **111**, 2518–2523 (2014).
22. Kasperkiewicz, P., Altman, Y., D'Angelo, M., Salvesen, G. S. & Drag, M. Toolbox of fluorescent probes for parallel imaging reveals uneven location of serine proteases in neutrophils. *J. Am. Chem. Soc.* **139**, 10115–10125 (2017).
23. Rut, W., Poreba, M., Kasperkiewicz, P., Snipas, S. J. & Drag, M. Selective substrates and activity-based probes for imaging of the human constitutive 20S proteasome in cells and blood samples. *J. Med. Chem.* **61**, 5222–5234 (2018).
24. Poreba, M. et al. Selective imaging of cathepsin L in breast cancer by fluorescent activity-based probes. *Chem. Sci.* **9**, 2113–2129 (2018).
25. Poreba, M. et al. Small molecule active site directed tools for studying human caspases. *Chem. Rev.* **115**, 12546–12629 (2015).
26. Maluch, I., Czarna, J. & Drag, M. Applications of unnatural amino acids in protease probes. *Chem.- Asian J.* **14**, 4103–4113 (2019).
27. Poreba, M. et al. Potent and selective caspase-2 inhibitor prevents MDM-2 cleavage in reversine-treated colon cancer cells. *Cell Death Differ.* **26**, 2695–2709 (2019).

Methods

Reagents. The reagents used for solid-phase peptide synthesis were as follows: Rink amide resin (particle size 100–200 mesh, loading 0.74 mmol g^{-1}), all Fmoc-amino acids, *O*-benzotriazole-*N*,*N*,*N*′,*N*′-tetramethyluronium-hexafluorophosphate (HBTU), 2-(1-H-7-azabenzotriazol-1-yl)-1,1,3,3-tetramethyluronium hexafluorophosphate (HATU), piperidine, diisopropylcarbodiimide (DICI) and trifluoroacetic acid (TFA), purchased from Iris Biotech; anhydrous *N*-hydroxybenzotriazole (HOBt) from Creosauls; 2,4,6-collidine (2,4,6-trimethylpyridine), high-performance liquid chromatography- (HPLC-)grade acetonitrile, triisopropylsilane (TIPS) from Sigma-Aldrich and *N*,*N*-diisopropylethylamie (DIPEA) from VWR International. *N*,*N*-dimethylformamide (DMF), dichloromethane (DCM), methanol (MeOH), diethyl ether (Et_2O), acetic acid (AcOH) and phosphorus pentoxide (P_2O_5), obtained from Avantor. Designed substrates were purified by HPLC on a Waters M600 solvent delivery module with a Waters M2489 detector system using a semipreparative Wide Pore C8 Discovery column. The solvent composition was as follows: phase A (water:0.1% TFA) and phase B (acetonitrile:0.1% TFA). The purity of each compound was confirmed with an analytical HPLC system using a Jupiter 10 µm C4 300 Å column (250 × 4.6 mm). The solvent composition was as follows: phase A (water:0.1% TFA) and phase B (acetonitrile:0.1% TFA); gradient, from 5% B to 95% B over a period of 15 min. The purity of all compounds was ≥95%. The molecular weight of each substrate was confirmed by high-resolution mass spectrometry using a Waters LCT premier XE with electrospray ionization and a time-of-flight module.

Enzyme preparation. Gene cloning and recombinant production of the SARS-CoV and SARS-CoV-2 M^{pro} are described elsewhere[9,17].

Combinatorial library synthesis. Synthesis of H_2N-ACC-resin. ACC synthesis was carried out according to Maly et al.[28]. To a glass reaction vessel, 1 eq. (9.62 mmol, 13 g) of Rink AM resin was added and stirred gently once per 10 min in DCM for 1 h, then filtered and washed three times with DMF. Fmoc-group deprotection was performed using 20% piperidine in DMF (three cycles of 5, 5 and 25 min), filtered and washed with DMF each time (six times). Next, 2.5 eq. of Fmoc-ACC-OH (24.05 mmol, 10.64 g) was preactivated with 2.5 eq. HOBt monohydrate (24.05 mmol, 3.61 g) and 2.5 eq. DICI (24.05 mmol, 3.75 ml) in DMF and the slurry was added to the resin. The reaction mixture was shaken gently for 24 h at room temperature. After this time, the resin was washed four times with DMF and the reaction was repeated using 1.5 eq. of above reagents to improve the yield of ACC coupling to the resin. After 24 h, the resin was washed with DMF and the Fmoc protecting group was removed using 20% piperidine in DMF (5, 5 and 25 min), filtered and washed with DMF (six times).

Synthesis of H_2N-Gln(Trt)-ACC-resin. Here, 2.5 eq. Fmoc-Gln(Trt)-OH (24.05 mmol, 14.69 g) with 2.5 eq. HATU (24.05 mmol, 9.15 g) and 2.5 eq. collidine (24.05 mmol, 3.18 ml) in DMF were activated for 2 min and added to a filter cannula with 1 eq. (9.62 mmol) H_2N-ACC-resin, and the reaction was carried out for 24 h. Next, the resin was washed four times with DMF and the same reaction was performed again using 1.5 eq. of these reagents. After four DMF washes, the Fmoc protecting group was removed using 20% piperidine in DMF (5, 5 and 25 min). Subsequently, the resin was washed with DCM (three times) and MeOH (three times) and dried over P_2O_5.

Library synthesis. The synthesis of P2, P3 and P4 sublibraries is exemplified in detail with the P2 sublibrary. The P2 library consisted of 137 compounds where all of the natural amino acids (omitting cysteine) and a pool of unnatural amino acids were used at a defined position (in this case, the P2 position) and an isokinetic mixture of 19 amino acids (without cysteine, plus norleucine mimicking methionine) was coupled in the remaining positions (in case of the P2 sublibrary, positions P3 and P4 were occupied by an isokinetic mixture). Equivalent ratios of amino acids in the isokinetic mixture were defined based on their reported coupling rates. A fivefold excess (over the resin load) of the mixture was used. For fixed positions, 2.5 eq. of single amino acid was used. All reactions were performed with the use of the coupling reagents DICI and HOBt. For P2 coupling, the synthesis of the library was performed using a MultiChem 48-well synthesis apparatus (FlexChem from SciGene). To each well of the reaction apparatus, 1 eq. of dry H_2N-Gln(Trt)-ACC-resin (0.059 mmol, 80 mg) was added and stirred gently for 30 min in DCM, and then washed four times with DMF. In separate Eppendorf tubes, 2.5 eq. (0.15 mmol) Fmoc-P2-OH was preactivated with 2.5 eq. HOBt (0.15 mmol, 22.5 mg) and 2.5 eq. DICI (0.15 mmol, 23.55 µl) in DMF. Next, preactivated amino acids were added to wells of the apparatus containing H_2N-Gln(Trt)-ACC-resin, followed by 3 h of agitation at room temperature. Then, the reaction mixture was filtered, washed with DMF (four times) and the ninhydrin test was carried out to confirm P2-amino-acid coupling. Subsequently, Fmoc protecting groups were removed with the use of 20% piperidine in DMF (5, 5 and 25 min). For P3 and P4 position coupling, an isokinetic mixture for 48 portions was prepared from 18 Fmoc-protected natural amino acids (omitting cysteine; plus norleucine mimicking methionine; 19 amino acids in total). Next, 5 eq. of isokinetic mixture, 5 eq. HOBt (14.16 mmol, 2.13 g) and 5 eq. DICI (14.16 mmol, 2.22 ml) were diluted in DMF and preactivated for 3 min. The activated isokinetic mixture was added to each of 48 wells containing 1 eq. of H_2N-P2-Gln(Trt)-ACC-resin. After 3 h of gentle agitation, the slurry was filtered off and washed with DMF (four times). A ninhydrin test was carried out and the Fmoc protecting group was removed using 20% piperidine in DMF (5, 5 and 25 min). The same procedure was applied for the remaining compounds. The isokinetic mixture was added to prepare the P4 position in the same manner as for the P3 position. In the last step of the synthesis, N-terminal acetylation was performed; to prepare the mixture for 48 compounds, 5 eq. of AcOH (14.16 mmol, 807 µl), 5 eq. HBTU (14.16 mmol, 5.37 g) and 5 eq. DIPEA (14.16 mmol, 2.44 ml) in roughly 45 ml of DMF were added to a 50-ml falcon tube. After gentle stirring for 1 min, the mixture (roughly 800 µl) was added to each well in the reaction apparatus, containing the H_2N-Mix-Mix-P2-Gln(Trt)-ACC-resin, followed by gentle agitation for 30 min. Next, the resin was washed six times with DMF, three times with DCM, three times with MeOH and dried over P_2O_5. After completing the synthesis, peptides were cleaved from the resin with a mixture of cold TFA:TIPS:H_2O (%, v/v/v 95:2.5:2.5; 2 ml per well; 2 h, shaking once per 15 min). The solution from each well was collected separately and the resin was washed once with a portion of fresh cleavage solution (1 ml), followed by addition of diethyl ether (Et_2O, 14 ml) into falcon tubes with peptides in solution. After precipitation (30 min at −20 °C), the mixture was centrifuged and washed again with Et_2O (5 ml). After centrifugation, the supernatant was removed and the remaining white precipitate was dissolved in ACN/H_2O (v/v, 3/1) and lyophilized. The products were dissolved in dimethylsulfoxide to a final concentration of 10 mM and used without further purification. The synthesis of P3 and P4 sublibraries was performed in the same manner as described above; P3 and P4 sublibraries were synthesized by coupling fixed amino-acid residues to the P3 (isokinetic mixture coupled to P2 and P4) and P4 positions (isokinetic mixture coupled to P2 and P3).

Library screening. HyCoSuL screening was performed using a spectrofluorometer (Molecular Devices Spectramax Gemini XPS) in 384-well plates (Corning). The assay conditions were as follows: 1 µl of substrate and 49 µl of enzyme, which was incubated at 37 °C for 10 min in assay buffer (20 mM Tris, 150 mM NaCl, 1 mM EDTA, 1 mM DTT, pH 7.3). The final substrate concentration was 100 µM and the final enzyme concentration was 1 µM SARS-CoV and 0.6 µM SARS-CoV-2 M^{pro}, respectively. The release of ACC was measured for 45 min (excitation wavelength of 355 nm and emission wavelength of 460 nm) and the linear part of each progress curve was used to determine the substrate hydrolysis rate. Substrate specificity profiles were established by setting the highest value of relative fluorescence unit per second from each position as 100% and others were adjusted accordingly.

Kinetic analysis of substrates. Substrate screening was carried out in the same manner as the library assay. Substrate concentration was 5 µM, SARS-CoV M^{pro} was 0.3 µM and SARS-CoV-2 M^{pro} was 0.3 µM. Substrate hydrolysis was measured for 30 min using the following wavelengths: excitation, 355 nm and emission, 460 nm. The experiment was repeated three times. Results were presented as mean values with standard deviations. Kinetic parameters were assayed in 96-well plates (Corning). Wells contained 80 µl of enzyme in assay buffer (0.016–0.1 µM SARS-CoV-2 M^{pro}) and 20 µl of substrate at eight different concentrations ranging from 58.5 to 1,200 µM (0.44–7 µM for IQF substrates). ACC liberation was monitored for 30 min (excitation, 355 nm; emission, 460 nm). Each experiment was repeated at least three times. Kinetic parameters were determined using the Michaelis–Menten equation and GraphPad Prism software. Due to the precipitation of internally quenched fluorescence substrates in assay buffer, only the specificity constant (k_{cat}/K_M) was determined. When the $[S_0] << K_M$, the plot of v_i (the initial velocities) versus $[S_0]$ yields a straight line with the slope representing V_{max}/K_M, k_{cat}/K_M = slope/E (E, total enzyme concentration).

Determination of inhibition kinetics (k_{obs}/I) for inhibitors and ABPs. SARS-CoV-2 M^{pro} (75 nM) was preincubated in assay buffer (20 mM Tris, 150 mM NaCl, 1 mM EDTA, 1 mM DTT, pH 7.3) for 10 min at 37 °C. Then, the enzyme was added to wells containing seven different concentrations of inhibitor or probe (ranging from 3.9 to 20 µM) and 50 µM of substrate (QS1). The measurement was conducted for 30 min and repeated at least three times; k_{obs}/I was calculated as previously described[21].

SARS-CoV-2 M^{pro} labeling. SARS-CoV-2 M^{pro} (5, 10, 50, 100 or 200 nM) was incubated with different probe concentrations (50–2,500 nM) in assay buffer (20 mM Tris, 150 mM NaCl, 1 mM EDTA, 1 mM DTT, pH 7.3) for 15 or 30 min at 37 °C. Then 3× SDS/DTT was added, and the samples were boiled for 5 min at 95 °C and resolved on 4–12% Bis-Tris Plus 12-well gels at 30 µl samples per well. Electrophoresis was performed at 200 V for 29 min. Next, the proteins were transferred to a nitrocellulose membrane (0.2 µm, Bio-Rad) for 60 min at 10 V. The membrane was blocked with 2% BSA in Tris-buffered saline with 0.1% (v/v) Tween 20 (TBS-T) for 60 min at room temperature. The biotinylated ABP was detected with a fluorescent streptavidin Alexa Fluor 647 conjugate (1:10,000) in TBS-T with 1% BSA using an Azure Biosystems Sapphire Biomolecular Imager (lasers of 658 and 488 nm for Bodipy FL dye) and Azure Spot Analysis Software.

To perform a time-point analysis, SARS-CoV-2 M^{pro} (10 nM) was incubated with Bodipy-QS5-VS (2.5 µM) for different durations of time in the range from 1 to 60 min. Then the samples were boiled, and run on a gel. For electrophoresis, protein transfer to a nitrocellulose membrane and probe visualization were conducted in the same manner as described above.

SARS-CoV-2 M^{pro} labeling in cell lysates. HeLa and HEK-293T cells were cultured in Dulbecco's modified Eagle's medium (DMEM) supplemented with 10% fetal bovine serum, 2 mM L-glutamine and antibiotics (100 U ml^{-1} penicillin, 100 µg ml^{-1} streptomycin) in a humidified 5% CO_2 atmosphere at 37 °C. Approximately 1,200,000 cells were collected and washed three times with PBS. The cell pellet was lysed in buffer containing 20 mM Tris, 150 mM NaCl and 5 mM DTT, pH 8.0, using a sonicator. The cell lysate was centrifuged for 10 min, and the supernatant was collected. Twenty microliters of cell lysate was incubated with or without 30 µl of inhibitor Ac-QS1-VS and with or without SARS-CoV-2 M^{pro} (100 or 25 nM) for 30 min at 37 °C. Next, 50 µl of probes at different concentrations was added to the samples and they were incubated for 15 or 30 min at 37 °C. Then the samples were combined with 50 µl 3× SDS/DTT, boiled and run on a gel. Electrophoresis, protein transfer to a nitrocellulose membrane and probe visualization were conducted in the same manner as described above. β-actin was used as a loading control (Source Data Fig. 1).

Antiviral activity of Ac-Abu-DTyr-Leu-Gln-VS toward a SARS-CoV-2 strain in Huh7 cell culture. The human hepatoma cell line Huh7 (kindly provided by R. Bartenschlager, University of Heidelberg, Germany) was maintained in DMEM (Gibco catalog no. 41965-039) supplemented with 10% fetal bovine serum (FBS), 2% HEPES 1 M (Gibco catalog no. 15630106), 5 ml of sodium bicarbonate 7.5% (Gibco catalog no. 25080-060) 1% nonessential amino acids (NEAA Gibco catalog no. 11140050) and 1% penicillin-streptomycin 10,000 U ml^{-1} (Gibco catalog no. 15140148) in a humidified 5% CO_2 incubator at 37 °C. Assay medium, used for producing virus stocks and antiviral testing, was prepared by supplementing DMEM with 4% FBS, 2% HEPES 1 M, 5 ml of sodium bicarbonate 7.5 and 1% NEAA.

To quantify antiviral activity on Huh7 cells, we selected a SARS-CoV-2 virus strain that produces sufficient cytopathogenic effect (CPE) on this cell line. We started from passage 6 of the SARS-CoV-2 strain BetaCov/Belgium/GHB-03021/2020 (EPI ISL 407976, 3 February 2020) that has been described previously[29], and passaged this three additional times on Huh7 cells while selecting those cultures that showed most CPE. This resulted in a virus stock (passage 9) that confers full CPE on Huh7 (5.6×10^4 median tissue culture infectious dose ($TCID_{50}$) per ml) as well as on VeroE6 cells (1.8×10^7 $TCID_{50}$ per ml). The genotype of this virus stock shows four nucleotide changes as compared with the mother virus stock (P6) and these are currently being analyzed. None of the nucleotide changes occur in the part of the genome that encodes the 3C-like protease, validating this virus stock for testing protease inhibitors.

For antiviral testing, Huh7 cells were seeded in 96-well plates (Corning CellBIND 96-well Microplate catalog no. 3300) at a density of 6,000 cells per well in assay medium. After overnight growth, cells were treated with the indicated compound concentrations and infected with a multiplicity of infection of 0.005 $TCID_{50}$ per cell of the P9 virus (final volume of 200 µl per well in assay medium). On day 4 postinfection, differences in cell viability caused by virus-induced CPE or by compound-specific side effects were analyzed using MTS (3-(4,5-dimethylthiazol-2-yl)-5-(3-carboxymethoxyphenyl)-2-(4-sulfophenyl)-2H-tetrazolium, inner salt). For this, an MTS:phenazine methosulfate (PMS) stock solution (2 mg ml^{-1} MTS (Promega) and 46 µg ml^{-1} PMS (Sigma-Aldrich) in PBS at pH 6–6.5) was diluted 1:20 in MEM without phenol red (Gibco catalog no. 51200038). Medium was aspirated from wells of the test plates and 70 µl of MTS/PMS solution was added. After 0.5–1 h incubation at 37 °C, absorbance was measured at 498 nm. Cytotoxic effects caused by compound treatment alone were monitored in parallel plates containing mock-infected cells.

All virus-related work was conducted in the high-containment BSL3+ facilities of the KU Leuven Rega Institute (3CAPS) under licenses AMV 30112018 SBB 219 2018 0892 and AMV 23102017 SBB 219 2017 0589 according to institutional guidelines.

Crystallization of SARS-CoV-2 M^{pro} in complex with Biotin-PEG(4)-Abu-Tle-Leu-Gln-VS. The purified SARS-CoV-2 M^{pro} was concentrated to 23 mg ml^{-1}, mixed with Biotin-PEG(4)-Abu-Tle-Leu-Gln-VS at a molar ratio of 1:5 and the mixture was incubated at 4 °C overnight. The next day, the mixture was clarified by centrifugation at 12,000*g*, 4 °C and the supernatant was set for crystallization screening by using commercially available screening kits (PEGRx^T 1 and 2 (Hampton Research) and Morpheus HT-96 (Molecular Dimensions)). A Gryphon LCP crystallization robot (Art Robbins) was used for setting up the crystallization screens with the sitting-drop vapor-diffusion method at 18 °C, where 0.15 µl of protein solution and 0.15 µl of reservoir were mixed to equilibrate against 40 µl of reservoir solution.

Crystals were observed under several conditions in the two 96-well plates. The crystals were fished directly from the basic screening plates. The cryo-protectant consisted of mother liquor plus varied concentrations (5 to 20%) of glycerol, and 2 mM of the ABP. Subsequently, liquid nitrogen was used for flash-cooling the crystals before data collection.

Diffraction data collection and determination of the structure. Several diffraction datasets were collected at 100 K at the P11 beamline of PETRA III (DESY), using synchrotron radiation of wavelength 1.0332 Å and a Pilatus 6M detector (Dectris). For structure determination, a dataset was used that was collected using a crystal fished from the condition no. E7 of Morpheus HT-96 (0.12 M ethylene glycols (0.3 M diethylene glycol, 0.3 M triethylene glycol, 0.3 M tetraethylene glycol, 0.3 M pentaethylene glycol), 0.1 M buffer system 2 (1.0 M sodium HEPES, MOPS (acid), pH 7.5), pH 7.5, 30% precipitant mix 3 (20% v/v glycerol, 10% PEG 4000)).

XDSapp[30], Pointless[31,32] and Scala[31] (the last two from the CCP4 suite[33]) were used for processing and scaling the dataset. The space group was determined as $P6_122$ and the resolution limit was set at a Bragg spacing of 1.70 Å. The molecular replacement method was used for phase determination using the Molrep program[33,34] and the free-enzyme crystal structure of SARS-CoV-2 M^{pro} (PDB 6Y2E, ref. [9]) as the search model. The geometric restraints for the ABP were generated using the Jligand programe from the CCP4 suite[33,35]; the ABP was built into the F_o–F_c density by using the Coot software[36]. Structure refinement was performed with Refmac5 (refs. [33,36,37]). Ramachandran statistics after structure refinement are as follows: preferred region 97.0%, allowed region 3.0% and outlier region 0.0%. Statistics of diffraction data processing and model refinement are shown in Supplementary Table 4.

Patient-sample preparation. The study was approved by the Bioethics Committee of the Medical University of Lodz, Poland (no. RNN/114/20/KE). The study was conducted in compliance with good clinical practice guidelines and under the principles of the Declaration of Helsinki. The study participants or their parents provided written informed consent. Patients were hospitalized at the Central Medical University Hospital in Lodz (CUHL), Poland and from the Department of Infectious Diseases and Hepatology, Medical University of Lodz (DIDH), Poland, and were positive for RNA of SARS-CoV-2 in serial measurements of nasopharyngeal swabs (at least two consecutive measurements) with clinical symptoms of infection.

For the current study, two nasopharyngeal swabs were collected from each patient at the same time, one was subjected to RNA SARS-CoV-2 testing and the other was used for smear preparation for confocal laser scanning microscopy. Smears were performed on glass slides covered with polylysine (Thermo Fisher Scientific).

Clinical characteristics of one patient (P01) recruited at CUHL. P01, a 13-year old boy, presented with mild symptoms of COVID-19 infection and no need for respiration support or mechanical ventilation; no specific treatment was applied. Two nasopharyngeal swabs for M^{pro} activity were collected during routine clinical examination, at days 1 and 5 after COVID-19 diagnosis. Tests positive for SARS-CoV-2 RNA were obtained on days 1 and 5, the first negative test was on day 7.

Clinical characteristics of six patients recruited at DIDH. P01DZ, a 59-year old woman, presented with moderate symptoms of COVID-19 infection, was hospitalized on day 3 after diagnosis, treated with respiration support (oxygen 3 l min^{-1}, for 10 d) and no mechanical ventilation was needed. She was treated with dexamethasone, hydroxychloroquine, lopinavir and ritonavir. One nasopharyngeal swab for M^{pro} activity was collected on day 12 after COVID-19 diagnosis during routine clinical examination. Tests for SARS-CoV-2 RNA were positive on days 1, 3, 12 and the first negative test was on day 20.

P02JB, a 34-year old woman, presented with moderate to severe COVID-19 pneumonia, was hospitalized on day 1 after diagnosis, treated with respiration support (oxygen 3 l min^{-1}, for 20 d) and no mechanical ventilation was needed. She was treated with dexamethasone, hydroxychloroquine, remdesivir and vancomycin because of concomitant *Clostridium difficile* infection. One nasopharyngeal swab for M^{pro} activity was collected on day 10 after COVID-19 diagnosis during routine clinical examination. Tests for SARS-CoV-2 RNA were positive on days 1, 7, 10 and 14, the first negative test was obtained on day 21.

P03KB, a 36-year old man, presented with moderate symptoms of COVID-19 pneumonia, was hospitalized on day 1 after diagnosis, treated with respiration support (oxygen 3 l min^{-1}, for 6 d) and no mechanical ventilation was needed. He was treated with dexamethasone, hydroxychloroquine, lopinavir and ritonavir. One nasopharyngeal swab for M^{pro} activity was collected on day 10 after COVID-19 diagnosis during routine clinical examination. Tests for SARS-CoV-2 RNA were positive on days 1, 7, 10 and the first negative test was on day 12.

P04WA, a 69-year old woman, presented with moderate symptoms of COVID-19 pneumonia, was hospitalized on day 1 after diagnosis, with respiration support (oxygen 3 l min^{-1}, required at the time of article submission). She was treated with hydroxychloroquine, dexamethasone and ceftriaxone. One nasopharyngeal swab for M^{pro} activity was collected on day 5 after COVID-19 diagnosis during routine clinical examination. Tests for SARS-CoV-2 RNA were positive on days 1 and 5.

P05WM, a 72-year old man, presented with moderate symptoms of COVID-19 pneumonia, was hospitalized on day 1 after diagnosis, with respiration support (oxygen 3 l min^{-1}, required at the time of article submission). He was treated with hydroxychloroquine and dexamethasone. One nasopharyngeal swab for M^{pro}

activity was collected on day 5 after COVID-19 diagnosis during routine clinical examination. Tests for SARS-CoV-2 RNA were positive on days 1 and 5.

P06JM, a 34-year old man with moderate symptoms of COVID-19 pneumonia, was hospitalized on day 1 after diagnosis, no needs for respiration support or mechanical ventilation. He was treated with hydroxychloroquine and ceftriaxone. One nasopharyngeal swab for M^{pro} activity was collected on day 5 after COVID-19 diagnosis during routine clinical examination. Tests for SARS-CoV-2 RNA were positive on days 1 and 5.

Detection of SARS-CoV-2 M^{pro} in epithelial cells by immunofluorescence. The nasopharyngeal swab was used for smear preparation for confocal laser scanning microscopy. Smears were performed on glass slides covered with polylysine (Thermo Fisher Scientific). These slides were treated with 1 or 2.5 µM probe of M^{pro} (Cy5-QS1-VS or Bodipy-QS5-VS) and incubated for 30 min at 37 °C. Slides were fixed in 70% ethanol for 30 min. For further staining overnight at 4 °C, incubation with recombinant goat anti-ACE2 antibody (R&D Systems, 1:20) was performed. The next day, antibodies were aspirated, and cells were washed twice with PBS and labeled with a secondary antibody (Donkey anti-Goat IgG (H+L) Highly Cross-Adsorbed Secondary Antibody, Alexa Fluor Plus 488 (catalog no. A32814, 1:200 Invitrogen, Thermo Fisher Scientific) or Cy5 AffiniPure donkey anti-Goat IgG (H+L) (705-175-147, 1:200, Jackson ImmunoResearch)) in PBS for 1 h at room temperature. Next, the cells were washed twice with PBS, coverslips were mounted with Vectashield fluorescence mounting medium containing 4′,6-diamidino-2-phenylindole (DAPI) (Vector Laboratory H-1000) and sealed with nail polish. Slides were stored at 4 °C until use. Cells were then subjected to confocal microscopy analysis using a Leica TCS SP8. DAPI was detected by the DAPI channel (405 nm), the M^{pro} Cy5-QS1-VS probe was detected with the Cy5 filter single photon laser (638 nm) (Bodipy-QS5-VS 488 nm) and ACE2/secondary antibodies were read using the fluorescein isothiocyanate filter (single photon laser 458 nm) or Cy5 filter laser 638 nm. All images were acquired in .tiff format using Leica Application Suite X software. Images shown are representative views of cells from two coverslips.

Slides with inhibitor (Ac-QS1-VS) were prepared in the same manner as described above. Cells were treated with 50 µM Ac-QS1-VS and incubated for 30 min at 37 °C. Then cells were washed twice with PBS and incubated with 2.5 µM Bodipy-QS5-VS for 30 min at 37 °C.

Reporting Summary. Further information on research design is available in the Nature Research Reporting Summary linked to this article.

Data availability

The authors declare that the main data supporting the findings of this study are available within the article and its Supplementary Information files. The expression plasmid for the SARS-CoV-2 main protease is available from R.H. (rolf.hilgenfeld@uni-luebeck.de). The atomic coordinates and structure factors for the complex between the SARS-CoV-2 M^{pro} and the ABP have been deposited in the Protein Data Bank under code 6Z2E. Source data are provided with this paper.

References

28. Maly, D. J. et al. Expedient solid-phase synthesis of fluorogenic protease substrates using the 7-amino-4-carbamoylmethylcoumarin (ACC) fluorophore. *J. Org. Chem.* **67**, 910–915 (2002).
29. Boudewijns, R. et al. STAT2 signaling as double-edged sword restricting viral dissemination but driving severe pneumonia in SARS-CoV-2 infected hamsters. Preprint at *bioRxiv* https://doi.org/10.1101/2020.04.23.056838 (2020).
30. Krug, M., Weiss, M. S., Heinemann, U. & Mueller, U. XDSAPP: a graphical user interface for the convenient processing of diffraction data using XDS. *J. Appl. Crystallogr.* **45**, 568–572 (2012).
31. Evans, P. Scaling and assessment of data quality. *Acta Crystallogr. D. Struct. Biol.* **62**, 72–82 (2006).
32. Evans, P. R. An introduction to data reduction: space-group determination, scaling and intensity statistics. *Acta Crystallogr. D. Biol. Crystallogr.* **67**, 282–292 (2011).
33. Winn, M. D. et al. Overview of the CCP4 suite and current developments. *Acta Crystallogr. D. Struct. Biol.* **67**, 235–242 (2011).
34. Vagin, A. & Teplyakov, A. Molecular replacement with MOLREP. *Acta Crystallogr. D. Biol. Crystallogr.* **66**, 22–25 (2010).
35. Lebedev, A. A. et al. JLigand: a graphical tool for the CCP4 template-restraint library. *Acta Crystallogr. D. Struct. Biol.* **68**, 431–440 (2012).
36. Emsley, P., Lohkamp, B., Scott, W. G. & Cowtan, K. Features and development of Coot. *Acta Crystallogr. D. Biol. Crystallogr.* **66**, 486–501 (2010).
37. Murshudov, G. N. et al. REFMAC5 for the refinement of macromolecular crystal structures. *Acta Crystallogr. D. Struct. Biol.* **67**, 355–367 (2011).

Acknowledgements

The Drag laboratory is supported by the National Science Center in Poland and the 'TEAM/2017-4/32' project, which is conducted within the TEAM program of the Foundation for Polish Science cofinanced by the European Union under the European Regional Development Fund. Work in the Hilgenfeld laboratory was supported by the SCORE project of the European Union (grant agreement no. 101003627), by DZIF and by the Government of Schleswig-Holstein through its Structure and Excellence Fund, as well as by a close partnership between the Possehl Foundation (Lübeck) and the University of Lübeck. Work in the Neyts laboratory was similarly supported by the SCORE project of the European Union (grant agreement no. 101003627). X.W. received funding of the China Scholarship Council (grant no. 201806170087). L.Z. is supported by a stipend from DZIF. W.R. is a beneficiary of a START scholarship from the Foundation for Polish Science. The Mlynarski laboratory (B.P. and W.M.) is supported by the FIXNET project, which is conducted within the TEAM-NET program of the Foundation for Polish Science cofinanced by the European Union under the European Regional Development Fund (no POIR.04.04.00-00-1603/18). We thank A. Piekarska (Medical University of Lodz, Poland) for an expert consultation in clinical assessments of patients with COVID-19.

Author contributions

M.D. and W.R. designed the research. W.R., K.G., L.Z., X.W., D.J. and M.Z. performed the research and collected data. R.H., X.S. and L.Z. contributed enzymes. L.Z. and R.H. solved and refined the crystal structure. B.P. and W.M. carried out labeling experiments in patient samples and confocal imaging. W.R., L.Z., W.M., X.W., D.J., J.N., R.H. and M.D. analyzed and interpreted the data. W.R., L.Z., R.H. and M.D. wrote the paper. All authors critically revised the paper.

Competing interests

Wroclaw University of Science and Technology has filed a patent application covering the compounds Ac-Abu-Tle-Leu-Gln-VS, Ac-Abu-ᴅTyr-Leu-Gln-VS, Biotin-PEG(4)-Abu-Tle-Leu-Gln-VS and Cy5-PEG(4)-Abu-Tle-Leu-Gln-VS as well as related compounds with W.R. and M.D. as inventors.

Additional information

Extended data is available for this paper at https://doi.org/10.1038/s41589-020-00689-z.

Supplementary information is available for this paper at https://doi.org/10.1038/s41589-020-00689-z.

Correspondence and requests for materials should be addressed to W.R. or M.D.

Reprints and permissions information is available at www.nature.com/reprints.

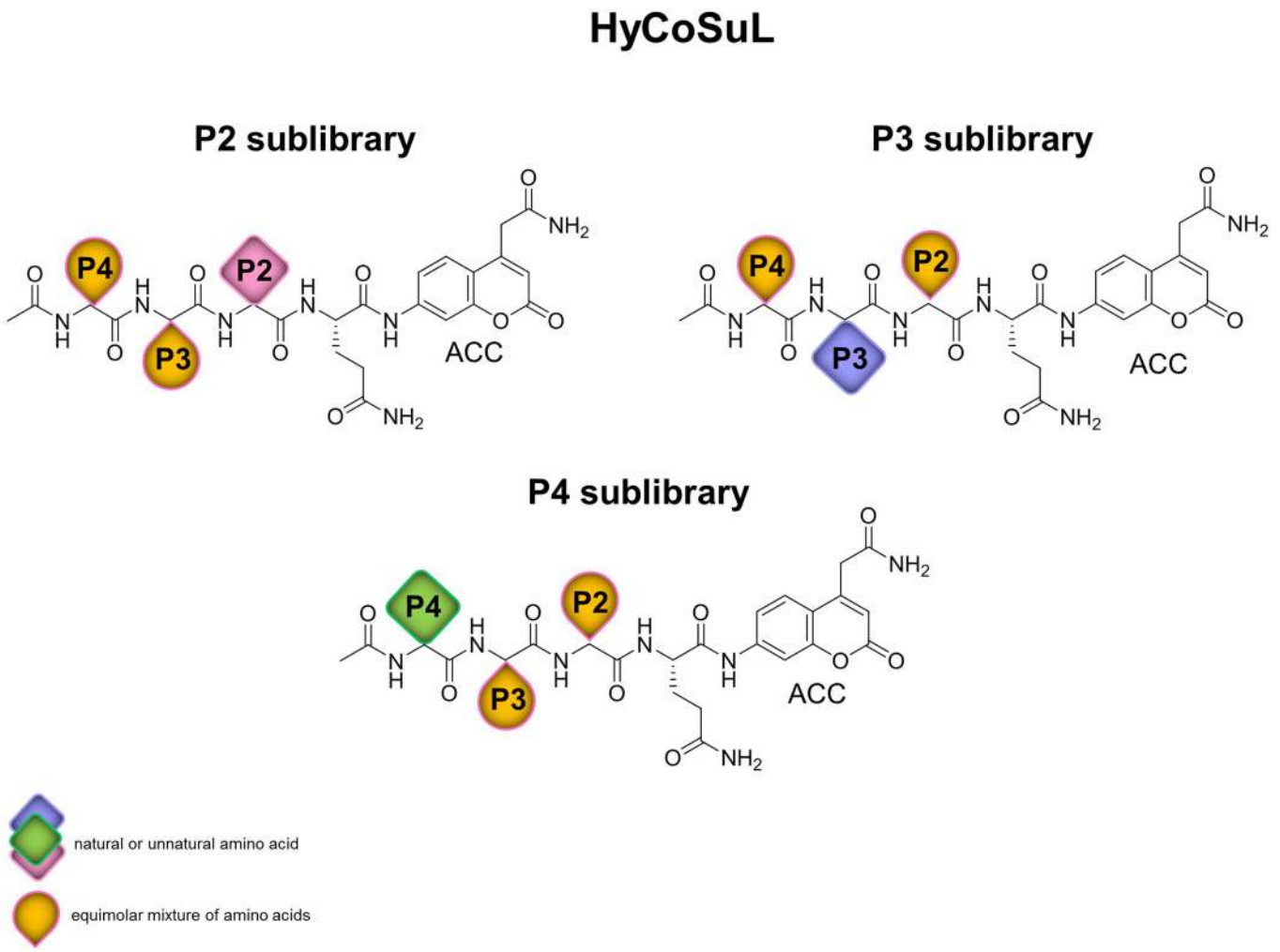

Extended Data Fig. 1 | The general library structure. Structure of HyCoSuL library designed for P1-Gln-specific endopeptidases.

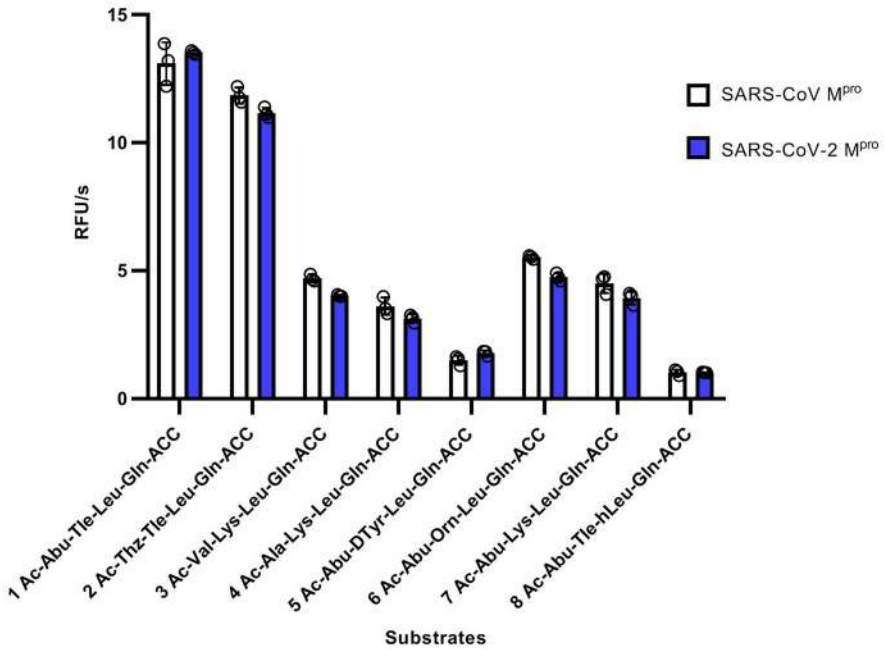

Extended Data Fig. 2 | The rate of substrate hydrolysis by SARS-CoV M^{pro} and SARS-CoV-2 M^{pro}. [S]=5 μM, [E]=0.3 μM; n=3, where n represents the number of independent experiments. Error bars represent mean ± SD.

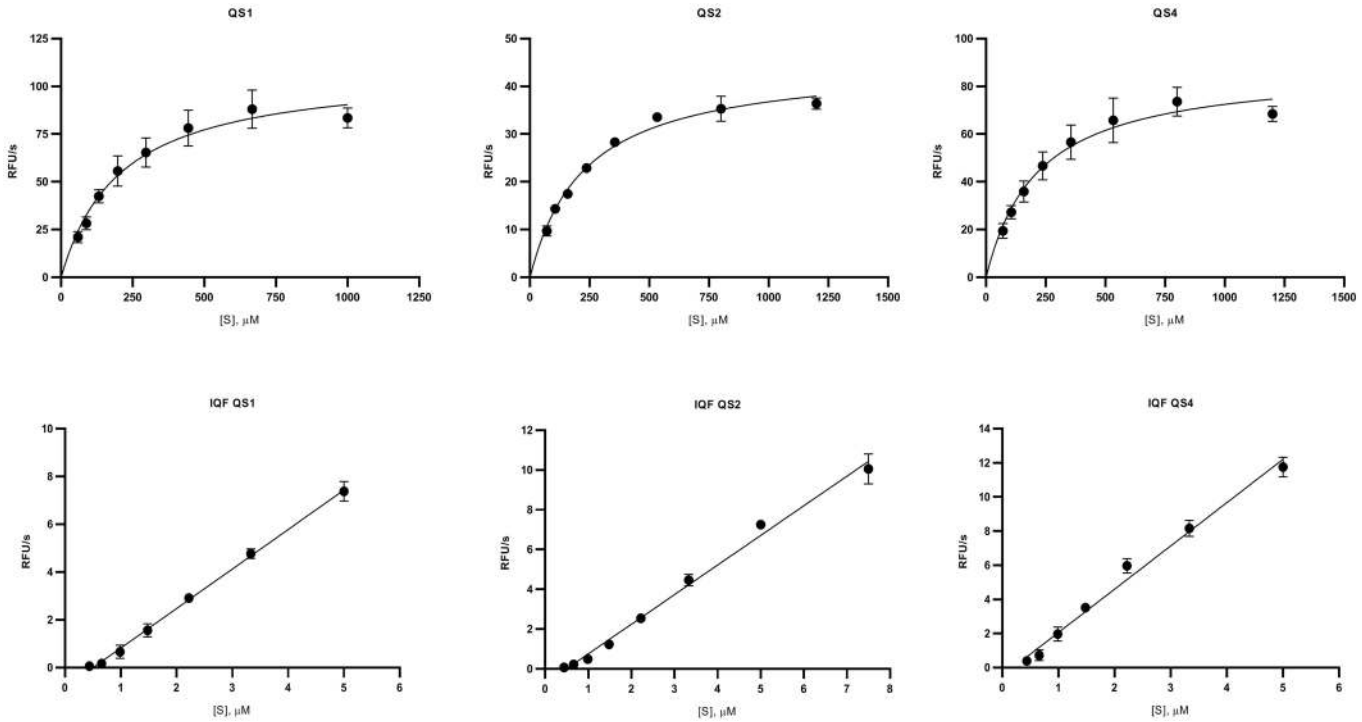

Extended Data Fig. 3 | Kinetic measurements of SARS-CoV-2 M^{pro} substrates. The measurements were performed in three independent replicates. Data are presented as mean values +/- SD. Due to internally quenched fluorescence substrate precipitation (IQF QS1, QS2 and QS4) in assay buffer only specificity constant could be determined.

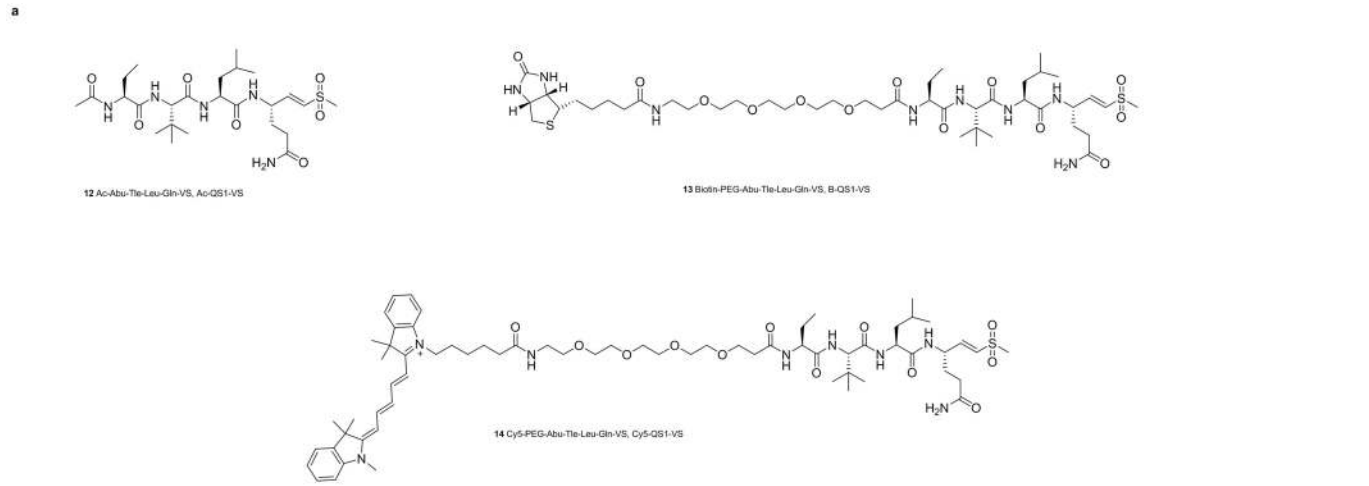

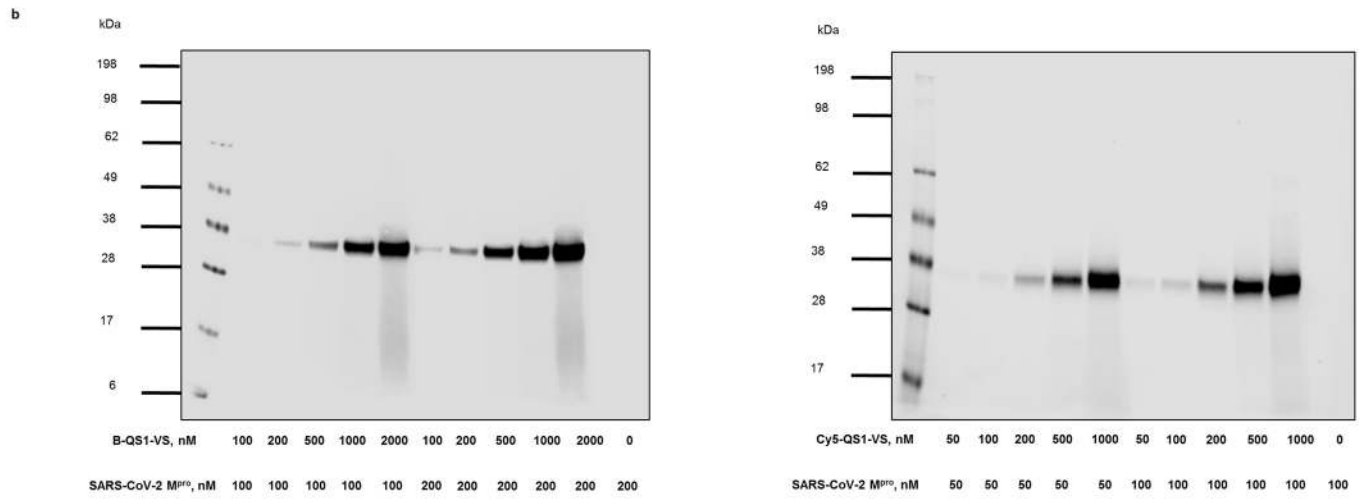

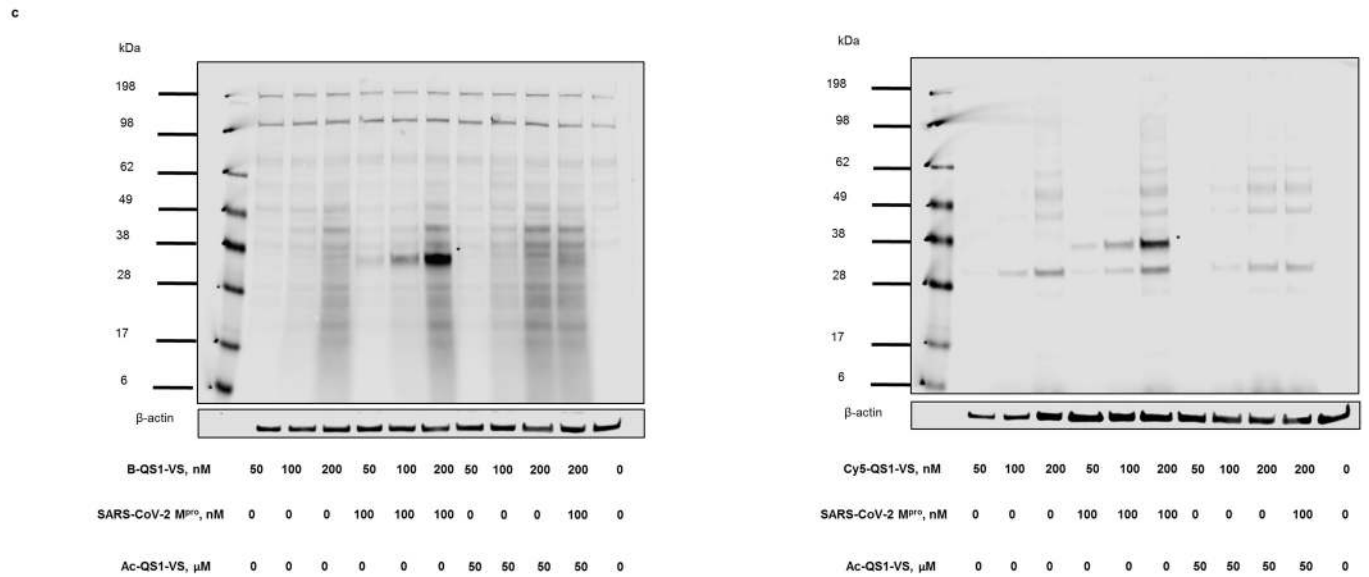

Extended Data Fig. 4 | See next page for caption.

Extended Data Fig. 4 | SARS-CoV-2 M^{pro} detection by activity-based probes. a, Structure of inhibitor and activity-based probes. **b,** SARS-CoV-2 M^{pro} labelling by probes (B-QS1-VS and Cy5-QS1-VS). **c**, SARS-CoV-2 M^{pro} probe selectivity in HeLa lysate (asterisk shows SARS-CoV-2 M^{pro} band, which was spiked into the cell lysate). The cell lysate was incubated with or without the inhibitor Ac-QS1-VS for 30 min at 37 °C; next, the different probe concentrations were added and the samples were incubated for 15 min at 37 °C. The biotinylated activity-based probe was detected with a fluorescent streptavidin Alexa Fluor 647 conjugate (1:10,000) in TBS-T with 1% BSA using an Azure Biosystems Sapphire Biomolecular Imager and Azure Spot Analysis Software. The last lane on the membranes is HeLa lysate only. Each experiment was repeated independently two times with similar results.

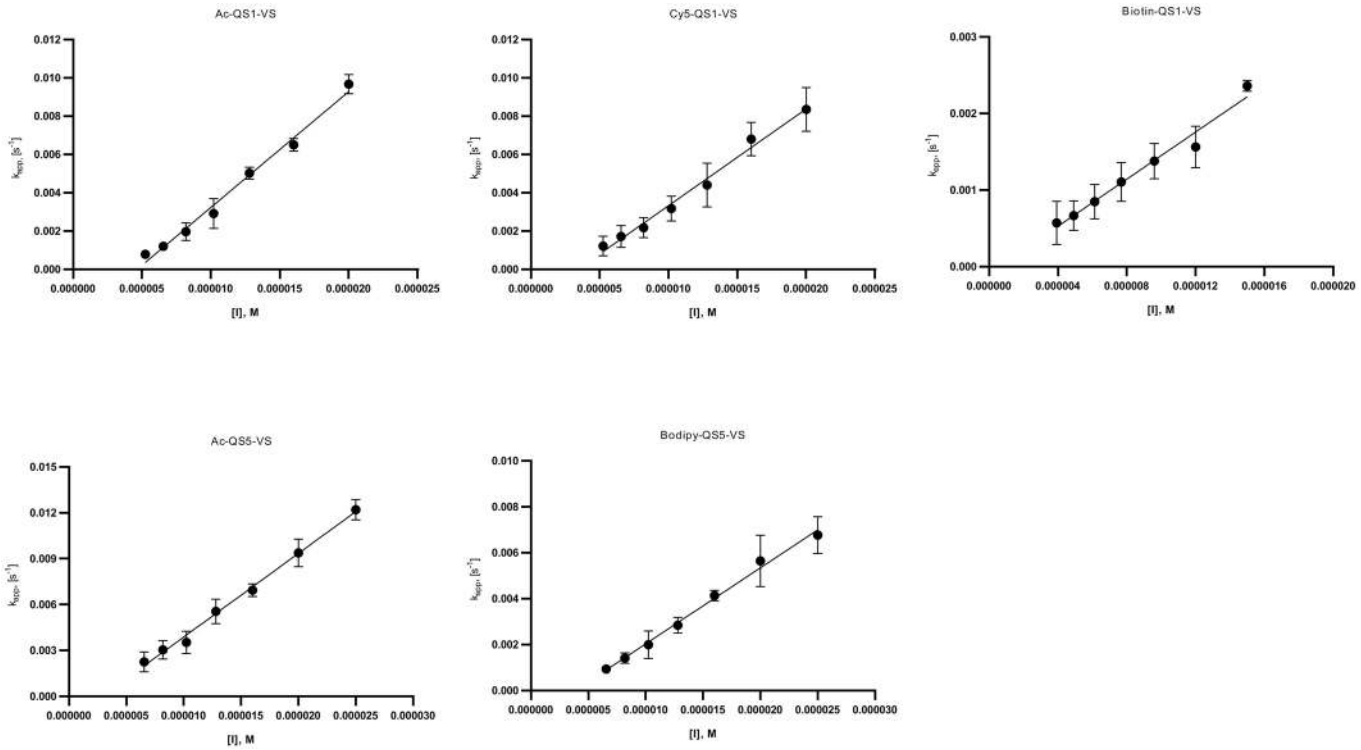

Extended Data Fig. 5 | Kinetic measurement of SARS-CoV-2 M^{pro} inhibitors and activity-based probes. Product formation (P) proceeded at an initial velocity (V) and was inhibited over time (t) at a rate of (k_{app}): $P=V/k_{app}*(1-e^{-kapp*t})+C$ (k_{app}– is the apparent rate of inhibition in the presence of substrate). k_{app} was determined separately for each inhibitor/probe concentration using non-linear regression analysis in GraphPad Prism software. The obtained values were plotted against inhibitor/probe concentration giving k_{app}/I (apparent second order rate constant). k_{obs}/I (absolute value of the second order rate constant) was calculated from $k_{obs}/I = k_{app}/I * (1+[S]/K_M)$. The measurements were performed in three independent replicates. Data are presented as mean values +/- SD.

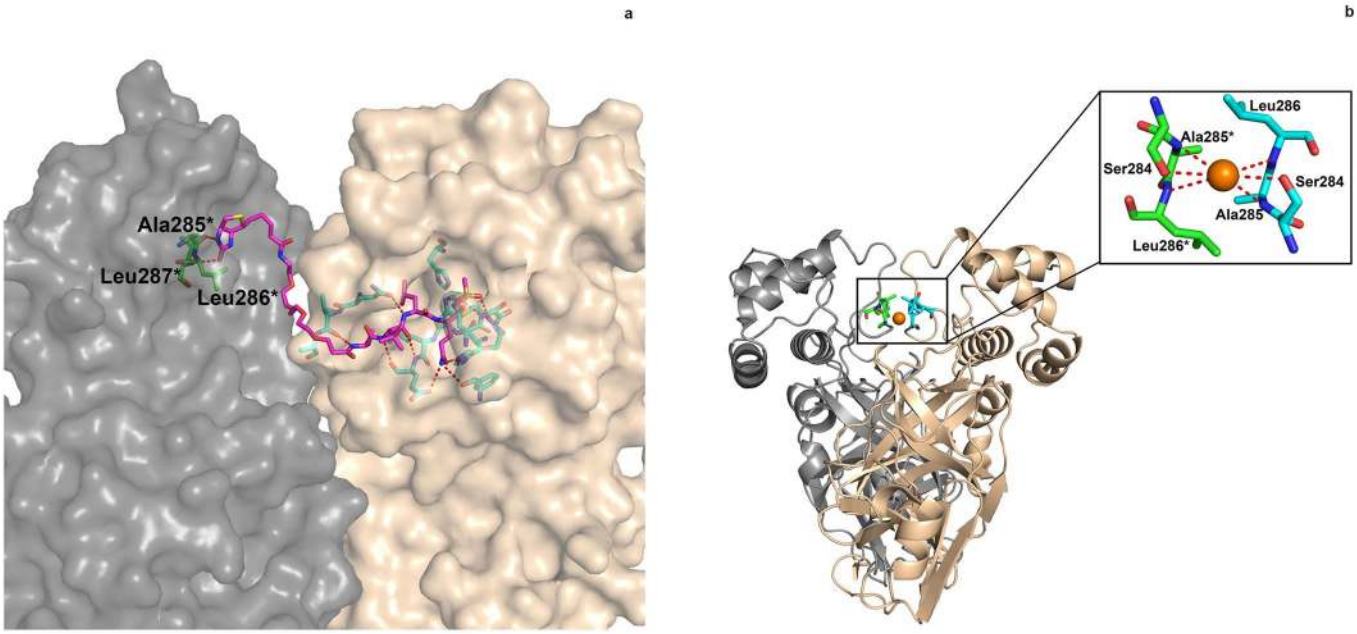

Extended Data Fig. 6 | Three-dimensional structure of the activity-based probe (ABP) Biotin-PEG(4)-Abu-Tle-Leu-Gln-VS (B-QS1-VS) in complex with the SARS-CoV-2 M^{pro}. a, In the crystal, the ABP links two neighboring M^{pro} dimers. The vinylsulfone warhead and the P1 - P4 residues bind to the substrate-binding site of the parent M^{pro} dimer (wheat), while the PEG(4) unit and the biotin label are in contact with the neighboring M^{pro} dimer (grey). **b**, At the monomer - monomer interface of the M^{pro}, a chloride ion from the crystallization buffer occupies a position on the two-fold axis.

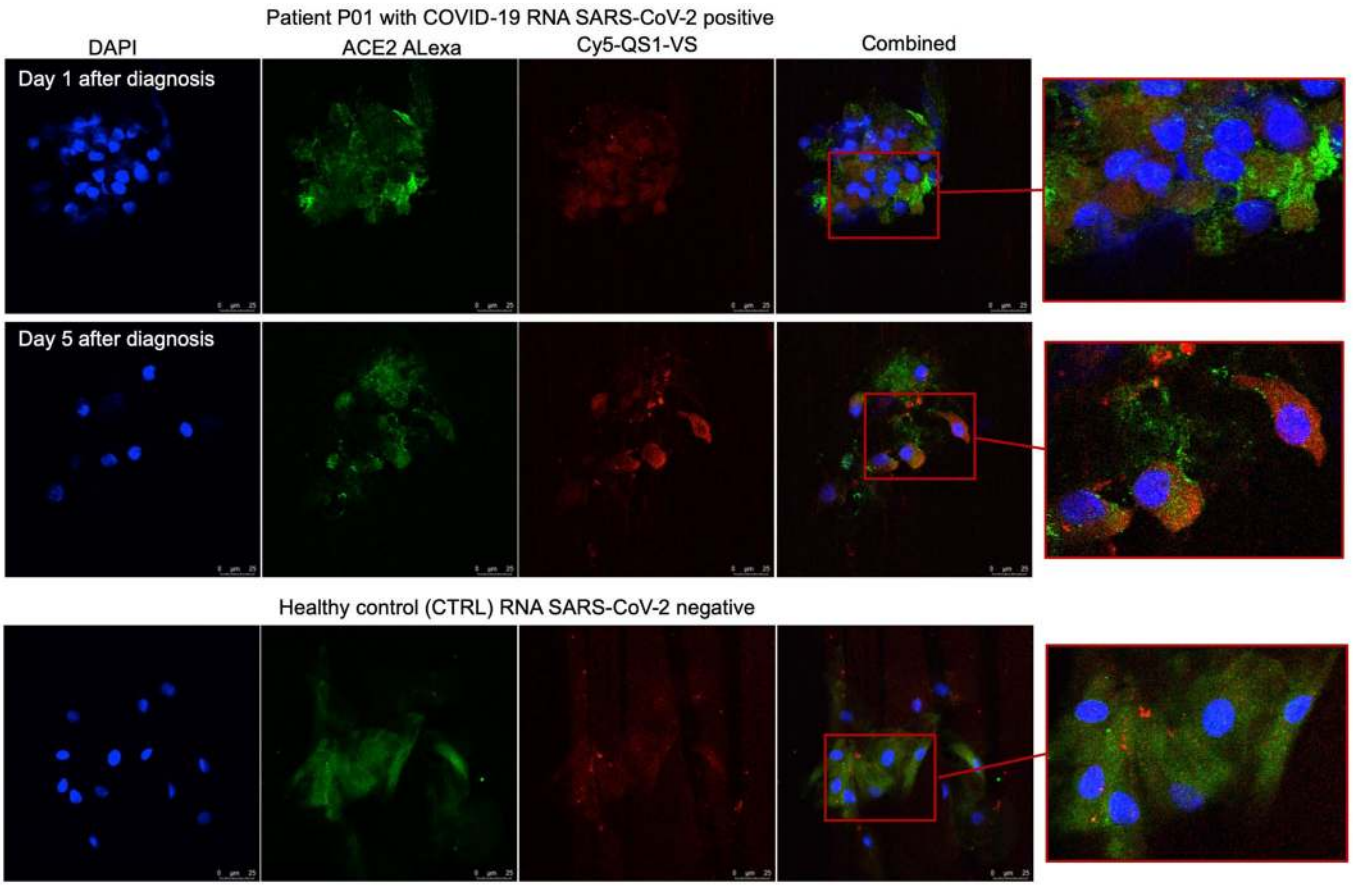

Extended Data Fig. 7 | SARS-CoV-2 M^{pro} detection by the activity-based probe in nasopharyngeal epithelial cells from COVID-19 patients positive for SARS-CoV-2 RNA (P01). Confocal microscopy of the epithelial cells of nasopharyngeal swabs co-stained with the Cy5-QS1-VS SARS-CoV-2 M^{pro} probe, anti-ACE2 antibody (ACE2 - angiotensin-converting enzyme 2) with Alexa Fluor 488 donkey anti-Goat secondary antibody, and DAPI (4′,6-diamidino-2-phenylindole) in patient P01 at days 1 and 5 after diagnosis as well as in a healthy control. Due to ethical concerns one nasopharyngeal swab was collected from patient P01 on day 1 and day 5.

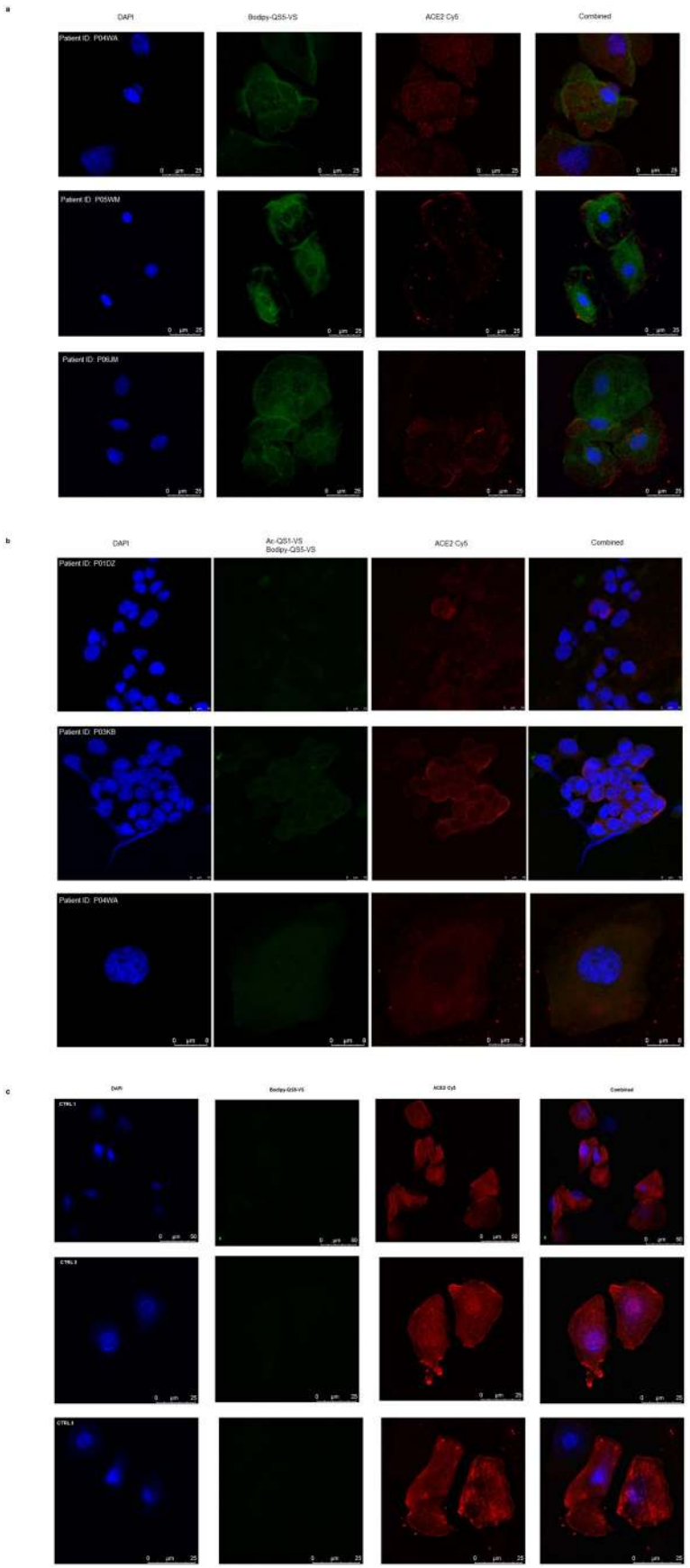

Extended Data Fig. 8 | See next page for caption.

Extended Data Fig. 8 | SARS-CoV-2 M^{pro} detection by the activity-based probe (Bodipy-QS5-VS) in nasopharyngeal epithelial cells from patients positive (panel a, b) and negative for SARS-CoV-2 RNA (CTRL 1-3, panel c). Confocal microscopy of the epithelial cells of nasopharyngeal swabs co-stained with Bodipy-QS5-VS SARS-CoV-2 M^{pro} probe and anti-ACE2 antibody with Cy5 AffiniPure donkey anti-Goat secondary antibody and DAPI. Panel b - cells were treated with 50 μM Ac-QS1-VS and incubated for 30 min at 37 °C. Then cells were washed twice with PBS and incubated with 2.5 μM Bodipy-QS5-VS for 30 min at 37 °C. Due to ethical concerns one nasopharyngeal swab was collected from each patient.

nature research

Corresponding author(s): Marcin Drag, Wioletta Rut

Last updated by author(s): Sep 28, 2020

Reporting Summary

Nature Research wishes to improve the reproducibility of the work that we publish. This form provides structure for consistency and transparency in reporting. For further information on Nature Research policies, see our Editorial Policies and the Editorial Policy Checklist.

Statistics

For all statistical analyses, confirm that the following items are present in the figure legend, table legend, main text, or Methods section.

n/a	Confirmed
☐	☒ The exact sample size (*n*) for each experimental group/condition, given as a discrete number and unit of measurement
☐	☒ A statement on whether measurements were taken from distinct samples or whether the same sample was measured repeatedly
☒	☐ The statistical test(s) used AND whether they are one- or two-sided *Only common tests should be described solely by name; describe more complex techniques in the Methods section.*
☒	☐ A description of all covariates tested
☒	☐ A description of any assumptions or corrections, such as tests of normality and adjustment for multiple comparisons
☐	☒ A full description of the statistical parameters including central tendency (e.g. means) or other basic estimates (e.g. regression coefficient) AND variation (e.g. standard deviation) or associated estimates of uncertainty (e.g. confidence intervals)
☒	☐ For null hypothesis testing, the test statistic (e.g. *F*, *t*, *r*) with confidence intervals, effect sizes, degrees of freedom and *P* value noted *Give P values as exact values whenever suitable.*
☒	☐ For Bayesian analysis, information on the choice of priors and Markov chain Monte Carlo settings
☒	☐ For hierarchical and complex designs, identification of the appropriate level for tests and full reporting of outcomes
☒	☐ Estimates of effect sizes (e.g. Cohen's *d*, Pearson's *r*), indicating how they were calculated

Our web collection on statistics for biologists contains articles on many of the points above.

Software and code

Policy information about availability of computer code

Data collection	SoftMax Pro 7.0.3, Pointless 1.11.21, Scala version: 3.3.22, Molrep 11.7.02, CCP4 Interface 7.0.078.
Data analysis	GraphPad Prism 6.0h, AzureSpot 2.0 Analysis Software, Leica Application Suite X, XDSAPP 2.0, Coot 0.8.9.2, PyMOL 1.8.6.1, Adobe photoshop CC 2019 20.0.0 release.

For manuscripts utilizing custom algorithms or software that are central to the research but not yet described in published literature, software must be made available to editors and reviewers. We strongly encourage code deposition in a community repository (e.g. GitHub). See the Nature Research guidelines for submitting code & software for further information.

Data

Policy information about availability of data

All manuscripts must include a data availability statement. This statement should provide the following information, where applicable:

- Accession codes, unique identifiers, or web links for publicly available datasets
- A list of figures that have associated raw data
- A description of any restrictions on data availability

The authors declare that the main data supporting the findings of this study are available within the article and its Supplementary Information files. The expression plasmid for the SARS-CoV-2 main protease is available from Rolf Hilgenfeld (rolf.hilgenfeld@uni-luebeck.de). The atomic coordinates and structure factors for the complex between the SARS-CoV-2 Mpro and the activity-based probe have been deposited in the Protein Data Bank under code 6Z2E.

Field-specific reporting

Please select the one below that is the best fit for your research. If you are not sure, read the appropriate sections before making your selection.

☒ Life sciences ☐ Behavioural & social sciences ☐ Ecological, evolutionary & environmental sciences

For a reference copy of the document with all sections, see nature.com/documents/nr-reporting-summary-flat.pdf

Life sciences study design

All studies must disclose on these points even when the disclosure is negative.

Sample size	The study was approved by the Bioethics Committee of the Medical University of Lodz, Poland (# RNN/114/20/KE). The study was conducted in compliance with good clinical practice guidelines and under the principles of the Declaration of Helsinki. The study participants or their parents provided written informed consent. Patients were hospitalized at the Central Medical University Hospital in Lodz (CUHL), Poland, and from the Department of Infectious Diseases and Hepatology, Medical University of Lodz (DIDH), Poland, and were positive for RNA of SARS-CoV-2 in serial measurements of nasopharyngeal swabs (at least 2 consecutive measurements) with clinical symptoms of infection. Confirmatory design of the study with no statistical power and sample size calculation was subjected for local IRB evaluation and approval. Thus, this approach was applied in the study. Since 100% match was obtained among 7 positive RNA SARS-CoV-2 patients examined at two time-points and three negative controls examined at one time-point, no further experiments on the larger sample size were performed.
Data exclusions	No data were excluded from the analysis
Replication	For the current study, two nasopharyngeal swabs were collected from each patient at the same time, one was subjected for RNA SARS-CoV-2 testing and the other was used for smear preparation for confocal laser scanning microscopy. Smears were performed on glass slides covered with polylysine (Thermo Fisher Scientific, MA, USA). Blinded confocal microscopy operator actively searched for fluorescent labelled cells and took at least 5 pictures (median 7). These pictures were compared with clinical case/control status and 100% match was obtained.
Randomization	The confirmatory design of the study eliminated an applicability of randomization. Only biological samples (nasopharyngeal swabs) which were positive and negative RNA SARS-CoV-2 were post hoc subjected for confocal microscopy experiments.
Blinding	No blinding procedures, at the level of patients' recruitment and biological samples preparation, were performed because only individuals with positive or negative serial swabs for RNA SARS-CoV-2 (for patient and control group, respectively) were included in this confirmatory approach. The confocal microscopy operator, who searched for fluorescent labelled cells was provided with blinded microscopic slides.

Reporting for specific materials, systems and methods

We require information from authors about some types of materials, experimental systems and methods used in many studies. Here, indicate whether each material, system or method listed is relevant to your study. If you are not sure if a list item applies to your research, read the appropriate section before selecting a response.

Materials & experimental systems

n/a	Involved in the study
☐	☒ Antibodies
☐	☒ Eukaryotic cell lines
☒	☐ Palaeontology and archaeology
☒	☐ Animals and other organisms
☐	☒ Human research participants
☒	☐ Clinical data
☒	☐ Dual use research of concern

Methods

n/a	Involved in the study
☒	☐ ChIP-seq
☒	☐ Flow cytometry
☒	☐ MRI-based neuroimaging

Antibodies

Antibodies used

Goat Anti-Human ACE2 Antigen Affinity purified Polyclonal Antibody (Catalog # AF933, LOT HOK0320041, Biotechne, Minneapolis, MN, USA)

Donkey anti-Goat IgG (H+L) Highly Cross-Adsorbed Secondary Antibody, AlexaFluor Plus 488 (Catalog # A32814, LOT VA293145, Invitrogen, ThermoFisher Scientific, USA)

Cy5 AffiniPure Donkey Anti-Goat Polyclonal IgG (H+L) Secondary Antibody (Catalog # 705-175-147, LOT 122280, JacksonImmuno Research, UK)

ProLong Gold Antifade Reagent with DAPI (Catalog # P36935, LOT 2180257, Invitrogen, ThermoFisher Scientific, USA).

	Goat anti-Mouse IgG (H+L) secondary antibody Alexa Fluor Plus 488, Lot:TF266577 Invitrogen; beta-Actin (c4) sc-47778 mouse monoclonal IgG1, Lot:D0618 Santa Cruz Biotechnology
Validation	Goat Anti-Human ACE-2 (Catalog # AF933): Hoffman, M. et al. (2020) Cell. DOI: 10.1016/j.cell.2020.02.052, less than 1% cross-reactivity with recombinantg human ACE (company statement) beta-Actin (c4) sc-47778 mouse monoclonal IgG1 - https://datasheets.scbt.com/sc-47778.pdf

Eukaryotic cell lines

Policy information about cell lines

Cell line source(s)	HeLa and HEK-293T cell lines purchased from ATCC. Human hepatoma cell line Huh7 was provided by Ralf Bartenschlager, University of Heidelberg, Germany. VeroE6 cells were obtained from ATCC.
Authentication	The cell lines were not authenticated.
Mycoplasma contamination	HeLa and HEK-293T cell line were not tested for mycoplasma contamination.Huh7 and VeroE6 cells were tested and were free of mycoplasma.
Commonly misidentified lines (See ICLAC register)	No commonly misidentified cell lines were used in the study.

Human research participants

Policy information about studies involving human research participants

Population characteristics	Seven patients with clinical and laboratory signs of COVID-19 were subjected for the study (median and range of age 36 (13-72) years, male/female 4/3). Three heathly volunteers (negative for SARS-CoV-2 RNA in nasapharyngal swab, aged 28, 30, 48 years; male/female 2/1) served as controls for the study.
Recruitment	The study was approved by the Bioethics Committee of the Medical University of Lodz, Poland (# RNN/114/20/KE). The study was conducted in compliance with good clinical practice guidelines and under the principles of the Declaration of Helsinki. The study participants or their parents provided written informed consent. Patients were hospitalized at the Central Medical University Hospital in Lodz (CUHL), Poland, and from the Department of Infectious Diseases and Hepatology, Medical University of Lodz (DIDH), Poland, and were positive for RNA of SARS-CoV-2 in serial measurements of nasopharyngeal swabs (positive in at least 2 consecutive measurements) with clinical symptoms of infection. Three consecutive volunteers, who served as healthy controls, were recruited among the CUHL hospital employees during a routine SARS-CoV-2 monthly medical personnel screening. No specific bias was identified since patients and healthy controls were recruited by two independent medical assistants who are not involved in the study.
Ethics oversight	The Bioethics Committee of the Medical University of Lodz, Poland (decision # RNN/114/20/KE)

Note that full information on the approval of the study protocol must also be provided in the manuscript.